ORIGINAL PAPER

Analysis on Structural Characteristics of Grout and Rock Distribution in Complex Geological Mixtures after Grouting Reinforcement and Its Mechanical Strength

Zhuo Zheng[1] · Shucai Li[1] · Rentai Liu[1]

Abstract

Soil rock mixture (SRM) is a common geo-material, which usually needs to be treated by grouting reinforcement. The grouting effect is tied to the grouting method, grout property, and geological condition, which are difficult to be quantitatively analyzed. The main obstacle in developing a rigorous theory for evaluating the grouting effect is the heterogeneity of SRM. This paper aims at developing a preliminary theoretical model and an empirical formula for predicting the overall strength of grouted SRM based on the actual morphological structure of grout-rock skeleton and its heterogeneity. A discrete element model was established for analysis of grout vein structures and validation of the theoretical approach. Two morphological parameters called "grout vein uniformity" and "block-skeleton conversion ratio" were proposed to quantify the influence of spatial distribution of grout vein and rock blocks in grouted SRM. Finally, an empirical formula was established for estimating the uniaxial compressive strength of grouted SRM, with a complete description of rock conversion ratio as a function of grout proportion and rock proportion. The ability of the approach to capture the influence of the grouting effect was verified by comparing the predicted values with the numerical values and the laboratory test results of this study. The improvement of the mechanical property of the stratum can be quickly assessed according to the obtained correlations as a general rule. Specifically, the normalized UCS increases in a linear fashion over grout proportion at a rock-soil ratio between 0.6 and 0.8. However, the theoretical model may overestimate the strength when the rock-soil ratio is higher than 0.9. It is open to improvement by further studies for the systemization of a more rigorous and robust approach in estimating and accommodating the uncertainties when applied in grouting operation guidance in the real world.

Keywords Soil–rock mixture · Grouting reinforcement · Empirical equation · Compressive strength

1 Introduction

1.1 Definition and Basic Mechanical Property of SRM

Soil–rock mixture (SRM) is a common geo-material widely distributed in fault zone as an infill and in quaternary strata (Xu 2008). It is a highly heterogeneous medium composed of rock blocks with various sizes and a relative high strength and a fine grained soil matrix, which lacks self-stability and may cause huge geological hazard if not properly treated,

such as landslide and tunnel collapse (Han et al. 2011; Gao et al. 2018; Khorasani et al. 2019).

The mechanical behaviors of SRM have been studied for more than 30 years since Raymond et al. (1984) proposed the concept of "bimrock" for complex and mixed geological masses for the first time. One of the most important features of SRM or bimrock is sufficient strength and stiffness contrast between rock block and matrix. The strength of rock block has a limited influence on the overall strength of SRM since failure surfaces always pass tortuously around blocks or within the matrix when it is loaded. When the volumetric block proportions (VBPs) in a bimrock increase, the internal friction angle tends to increase and cohesion tends to decrease (Lindquist 1994; Lindquist and Goodman 1994). Kalender et al. (2014) developed an empirical formula for predicting the overall strength of SRM and bimrock, which considered fundamental rules of rock and soil mechanics

✉ Zhuo Zheng
413708318@qq.com

1 Geotechnical and Structural Engineering Research Center, Shandong University, Jinan 250061, China

and mechanical behaviors of bimrock as a function of VBP. Besides, the influence of the strength and shape of blocks on the overall strength of SRM and the failure patterns has also been investigated. Dong (2007) found that with an increase of the stiffness of rock blocks, the friction angle of the SRM became higher, while the cohesion became lower. SRM with angular blocks are characterized by a higher shear strength and a more pronounced dilatant response as compared to those containing rounded blocks (Hamidi et al. 2011; Jin et al. 2017). In addition, numerous researches have been carried out to fully understand mechanical behaviors and failure mechanisms of SRM, by means of in situ tests (Xu et al. 2007, 2011; Jiang and Yang 2010; Coli et al. 2011; Zhang et al. 2016a) and numerical tests (Coli et al. 2012; Xu et al. 2015, 2016a, 2018; b; Zhang et al. 2016b; Chen et al. 2018; Hu et al. 2018).

Due to its heterogeneity and lack of self-stability, SRM is usually regarded as an unfavorable geological condition in tunneling, mining and other underground constructions, especially when tunneling across fault zone, which may cause cave-in, TBM jamming, water and mud inrush and other engineering disasters (Shang et al. 2004; Li et al. 2016). Some other problems may also be caused during construction in quaternary strata, such as uncontrolled subsidence and inflow of groundwater during shallow buried tunneling and excavation of foundation pit (Li et al. 2016; Zhuo et al. 2020).

1.2 Grouting in SRM

Grouting is a widely used method for ground improvement and geological hazard control (Li et al. 2016). Successful grouting provides improved mechanical strength of formation, reduced permeability and compression of soft material. Flow patterns in a grouting work are mainly divided into two types, namely permeation grouting and fracturing grouting (Widmann 1996; Saada et al. 2005; Axelsson et al. 2009),

which depend on the geological conditions as well as the physical and rheological property of the grout. In an ideal condition that the formation is composed of homogeneous media like pure soil or porous rock, permeation grouting is the first choice, which is intended to fill cavities and pore spaces in soil or rock and voids in rock joint systems with cement suspensions or chemical solutions. During grouting, the grouts are assumed to diffuse uniformly in all directions, which can provide a permanent and uniform improvement of the formation after the grouts harden. The size of the diffusion region and its mechanical property after grouting reinforcement can easily be assessed by mathematical analysis.

In practical terms, this ideal process is always limited by heterogeneity of the formation and its low groutability. Specifically, when grouting in SRM using cement suspension, the mechanisms of grouting diffusion and reinforcement are much more complicated. Since the cement particles cannot go through the pore voids in the soil, fracturing occurs in the interior of the soil or along the soil–rock interface. Moreover, the flow path and the shape of the fractures in SRM are much more tortuous with multiple branches than those in pure soil or sand where a dominant planar fracture is more likely to form. Figure 1 summarizes the typical flow patterns when grouting in different media.

For a homogenous medium, the improvement on mechanical properties after grouting is proportional to the quantity of the grouts. Thus, it is not difficult to establish a functional relationship between them according to laboratory tests on artificial samples with different proportions of the soil and grouts completely mixed. In contrast, SRM is a highly heterogeneous medium, and its heterogeneity may become even more obvious after grouting. The mechanical strength of grouted SRM depends on the supporting skeleton composed of rock block and grout vein, while the contribution of soil matrix is trivial. When under external loading, failure occurs in the weakest regions of the skeleton, mainly on the thinnest part of the grout veins or on the rock–grout interface.
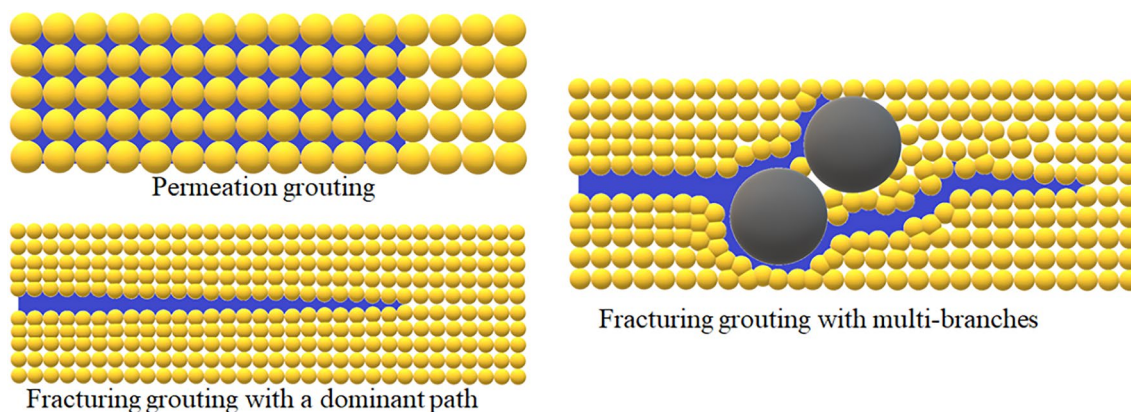

Fig. 1 Typical flow patterns when grouting in sand, clay and SRM

In the meantime, the rock blocks remain intact. The overall strength is controlled by the structural effect, rather than the own strengths of the grout and rock. In order to evaluate the grouting effect on SRM, a number of factors need to be considered, such as morphology of grout vein, grout and rock quantity, spatial relation between rock block and grout vein and adhesive strength on the interface.

1.3 Aim of This Paper

The strength and deformation properties of geological masses are crucial parameters for design and construction of engineering projects. The mechanical strength and stability of SRM can be markedly improved by grouting reinforcement. Unfortunately, researches on evaluating mechanical properties of grouted SRM are very limited, since the grouting effect is tied to the grouting method, grout property, and geological condition, which are difficult to be quantitatively analyzed. Currently, the success of grouting can only be assessed upon the termination of grouting and still largely depends on the practical experience of the designer. Only a few laboratory or field tests and some simplified theoretical analysis were conducted by assuming grouted SRM as a homogenous medium, which completely discarded the structural effect, while rigorous theoretically based criteria are still missing (Jin et al. 2016; Li et al. 2016).

This paper aims at developing a preliminary theoretical model and an empirical formula for predicting the overall strength of grouted SRM based on the actual morphological structure of grout-rock skeleton and its heterogeneity. For this aim, two morphological parameters, called "grout vein uniformity" and "block-skeleton conversion ratio", were proposed to quantify the influence of spatial distribution of grout vein and rock blocks in grouted SRM. An empirical formula was then established for estimating the uniaxial compressive strength (UCS) of grouted SRM. The ability of the approach to capture the influence of the supporting skeleton was verified by comparing the predicted values of SRM samples with artificial structures in terms of the morphological parameters and the measured values from a numerical simulation result based on the Particle Flow Code (PFC).

2 PFC Model Setup

In this study, a PFC model of SRM was established for analysis of grout vein structures and to provide UCS test data for verification of the theoretical approach. The reason that a laboratory test was not adopted is because the numerical model better captures the crucial factors which are consistent with those considered in the theoretical model, and because it is more convenient for the investigation. Although the accuracy of the prediction results of the theoretical approach is related to the calibration on its empirical parameters using the numerical test data, the development and the rationality of the theoretical approach are independent from the PFC model.

The constitutive relations of the contacts in the model and the calibration procedure in the model setup are quite simple, since the focus is not to reproduce mechanical behaviors of a specific rock in the real world. Herein, the parallel-bond model (PBM) (Potyondy and Cundall 2004) was adopted to characterize the cohesive forces both in the interior of soil, grout vein and rock block, and on their interface. Although some new constitutive models have been proposed in recent years (Nguyen et al. 2017; Saadat and Taheri 2019), which can mimic the mechanical behaviors of rock mass more precisely in some way, they are not adopted in the present model due to the increased number of micro-parameters and complexity for calibration.

The parallel bond provides the mechanical behavior of a finite-sized piece of cement-like material deposited between the particles. The force and moment act on the two contacting particles can be related to maximum normal and shear stresses acting within the bond material at the bond periphery. If either of these maximum stresses exceeds its corresponding bond strength, the parallel bond breaks and the bond material is removed from the model along with its accompanying force, moment and stiffness (Itasca Consulting Group 2016). Therefore, the cohesive softening response after the yield limit might be overlooked, since an abrupt reduction of contact forces to zero will occur when the contact forces exceed the bond strength. However, this error is deemed to be negligible.

Synthetic samples of grouted SRM were generated in a square region of 20 cm in length, comprising approximately 12,000 particles with a radius ranges from 0.8 mm to 1.2 mm. Grout vein and rock blocks in SRM sample are characterized by assigning a higher value of mechanical parameters than the soil matrix on particles in selected regions. Regions for grout vein are determined by importing geometric data representing grout vein boundaries which are obtained according to a hydro-fracturing simulation method (Zhuo et al. 2019). Since the influence of angularity of rock block is not considered in this study, regions for rock block are assumed to be circular. The average value of the diameter is 2.5 cm. During simulation, all the rock blocks kept their integrity, and no crush occurred on the inside. The micro-parameters are assigned in a reasonable range for common soil and rock according to the tutorials in PFC manual. Grout veins are given a value one order of magnitude lower than rock blocks. Since this numerical model is mainly used to provide data for verification of the theoretical approach, no calibration was conducted for adjusting these parameters to obtain macro-properties of a specific rock mass. The values of the micro-parameters are listed in Table 1.

Description	Symbol	Unit	Value (soil)	Value (grout)	Value (rock)
Density of the particle	ρ	kg/m^3	2500	2500	2500
Friction coefficient	μ	–	0.25	0.25	0.25
Normal stiffness	k_n	N/m	10^7	10^{10}	10^{11}
Shear stiffness	k_s	N/m	10^7	10^{10}	10^{11}
Porosity	n	–	0.1	0.1	0.1
Bond normal stiffness	$\overline{k}_n$	N/m	10^7	10^{10}	10^{11}
Bond shear stiffness	$\overline{k}_s$	N/m	10^7	10^{10}	10^{11}
Tensile strength	$\overline{\sigma}_n$	MPa	0.02	2	20
Cohesion	$\overline{c}$	MPa	0.02	2	20

3 Investigation on Morphology and Strength of Grout Vein Skeleton

3.1 Conceptualization and Definition of Grout Vein Uniformity

As mentioned in Sect. 1.2, a comprehensive evaluation on the mechanical strength of SRM after grouting reinforcement depends on a series of factors such as morphology of grout vein, grout and rock quantity, spatial relation between rock block and grout vein, and adhesive strength on the interface. In this section, the influences of rock block are temporarily not considered. The test samples only comprise a supporting skeleton of grout vein and soil matrix, and it is called grouted soil for convenience. The samples comprising soil, rock block and grout vein are called grouted SRM. "Grout proportion" refers to the volumetric ratio of the grout and the sum of grout and soil both for grouted soil and for grouted SRM throughout this paper. "Rock proportion" is particularly used for grouted SRM, which refers to the volumetric ratio of the rock and the sum of rock, grout and soil.

The overall geometry of a grout vein can be very complex with multiple branches and high tortuosity. Every tiny change in a local region will make the failure pattern different. Therefore, each sample with a grout vein skeleton has a particular stress path and macroscopic mechanical behavior (Fig. 2a). However, investigation on the failure patterns for each specific grout vein is impracticable. Herein, a statistical approach is used to analyze the morphological characteristics of grout vein. Grout proportions are the same in all these six samples. Perceptually, the two samples in each column have a similar distribution of soil and grout. To quantify the differences between the columns from each other, three observation regions with circular shape are randomly selected from the samples. Then, a variance of the grout proportions in each region is calculated. A smaller variance represents a higher homogeneity of distribution. Therefore, in order to obtain a precise value of the variance, a sufficient number of observation regions is needed.

Besides, the value of the variance is related to the scale of the observation region (Fig. 2b). For example, when the observation scale is close to the size of the sample, the variance is approaching zero regardless of the distribution of soil and grout, which means all these three samples are regarded as completely uniformly distributed. When the observation scale is reduced to half the size of the sample, the difference becomes obvious between sample 1 and the other two. The variances of samples 1 and 2 increase as the observation scale decreasing. However, the variance of sample 3 remains unchanged until the observation region is close to the grain scale (i.e.. the soil or cement particle size).

Since the value of the variance depends on the scale of the observation region, the morphological characteristics of grout vein cannot be represented using a single value from one specific scale. To fully consider the influence of the scale of the observation region, the following calculation approach was adopted (Fig. 3): assuming the length of the sample is l, and the length of the observation region is l_n, observation regions are fully distributed on the sample. The value of the variance of all these regions (S_n) is calculated as an observation of the nth order:

$$l_n = l/n \tag{1}$$

$$S_n = \frac{\sum_{i=1}^{n \cdot n} (p_i - p)^2}{n \cdot n}, \tag{2}$$

where p_i is the grout proportion in any observation region and p is the grout proportion of the whole sample.

To obtain a more general result, the influence of different grout proportions needs to be taken into account. Figure 4a shows two sample groups (sample 1 and 2; samples 3 and 4). Each of them has a similar heterogeneity of grout vein distribution. The grout proportion of sample 1 and sample 3 is 35%, while for sample 2 and sample 4 it is 50%. The S_n–n curves for each sample are presented in Fig. 4b.

In order to compare the samples with different grout proportions, the value of S_n needs to be normalized.

Fig. 2 Samples of grouted soil with different grout vein distributions
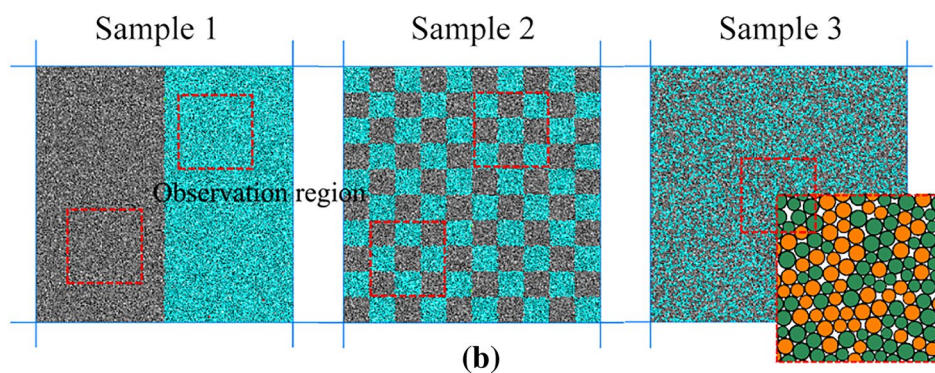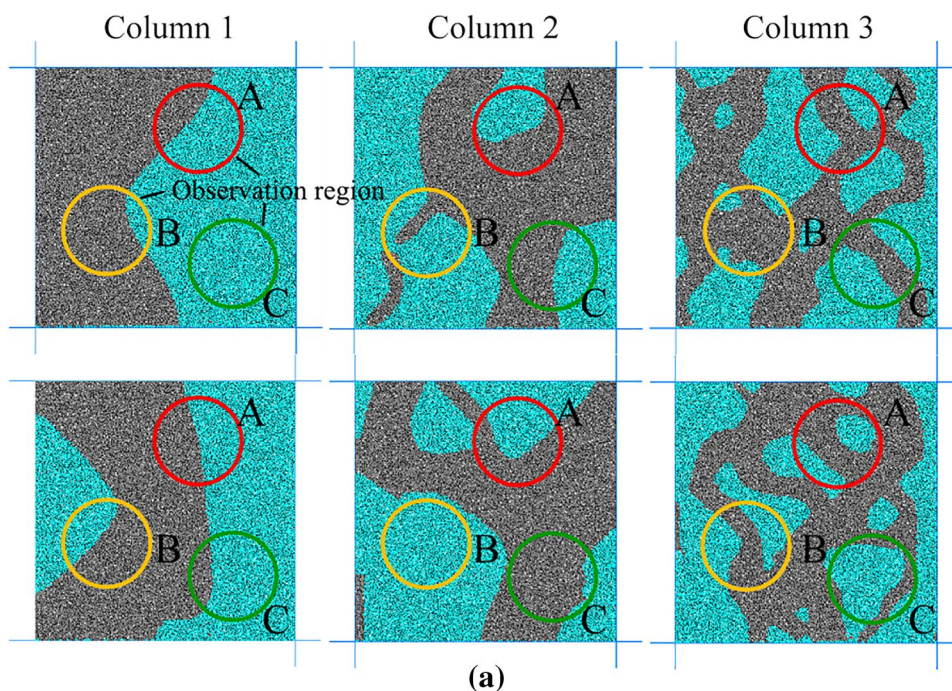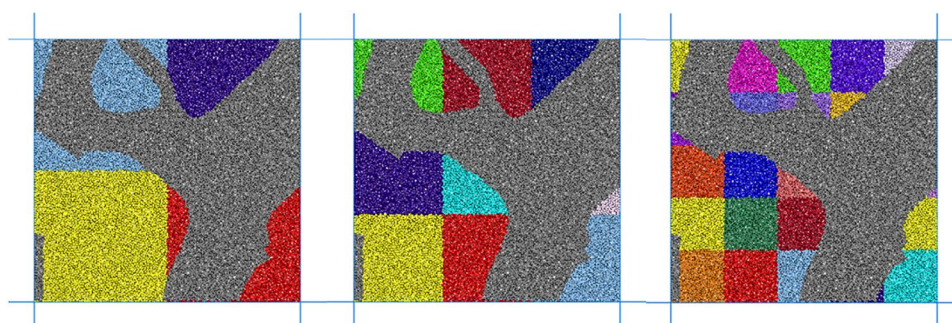

(a)

(b)

Fig. 3 The calculation procedure for the variance curve by dividing the observation regions into different scales (note that the colors are only used for differentiate the boundaries, not representing the actual variance in each region) (color figure online)

Actually, for a sample with any grout proportion p, when n is approaching infinity, S_n and p obey the following mathematical relation:

$$\lim_{n \to \infty} S_n = p \cdot (1 - p). \tag{3}$$

Therefore, the normalized variance of grout vein distribution can be expressed as follows:

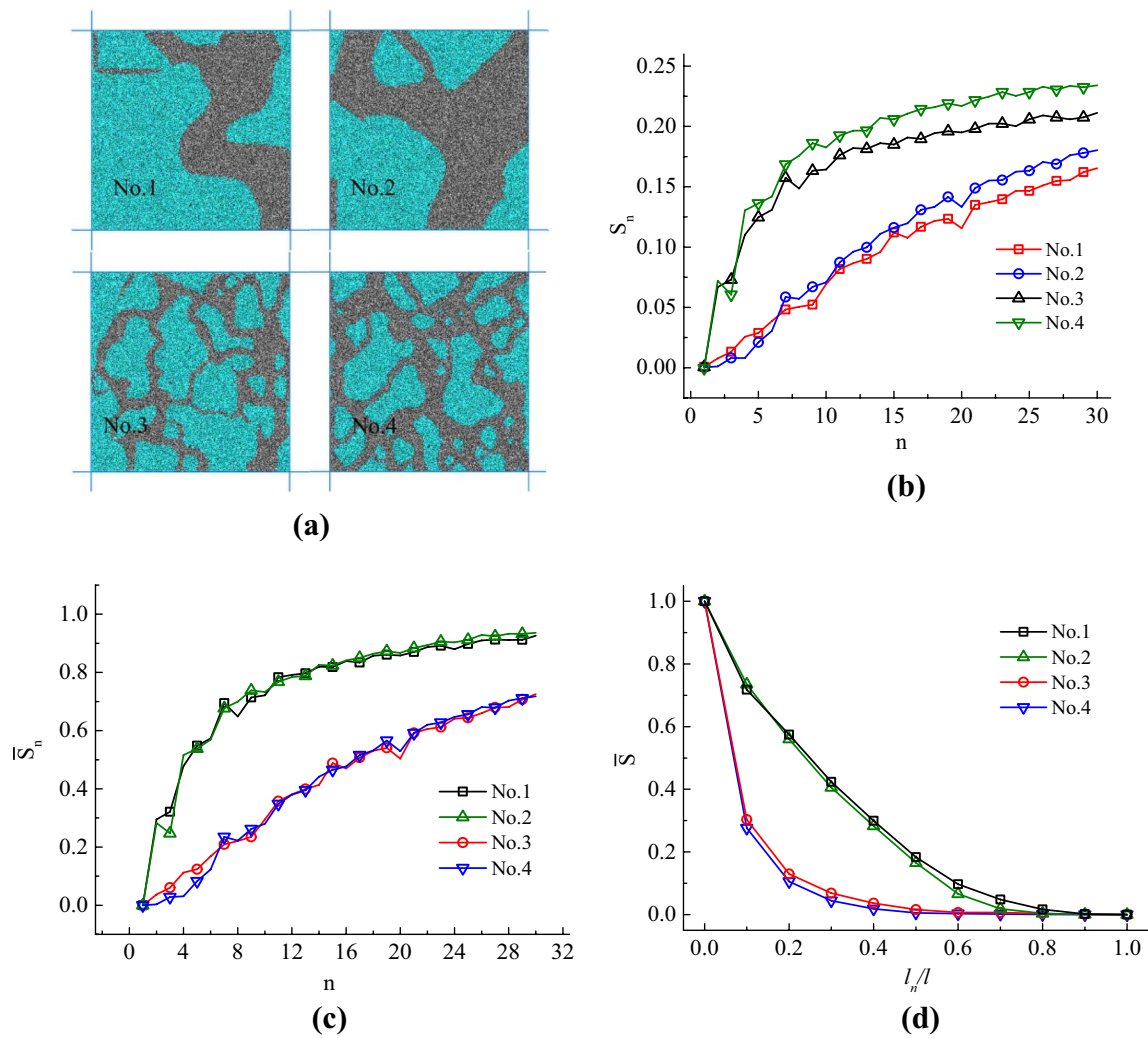$$\overline{S}_n = \frac{S_n}{p \cdot (1 - p)}. \tag{4}$$

Fig. 4 A generalized calculation procedure for grout vein uniformity by normalization with grout proportion and reorganization on the coordinates (**a** presents four samples which have the same grout vein heterogeneity for each line and the same grout proportions for each column; **b** presents the S_n–n curves of each sample; **c** presents the calculation results after normalization with grout proportion; **d** presents the calculation results after coordinate transformation and data redistribution.)

The curves in Fig. 4b can be recalculated with the normalized variance as shown in Fig. 4c.

Although the curve of S_n can reflect the heterogeneity of grout vein distribution, it is not convenient to use in the calculation of grouting reinforcement, and a more specific parameter is needed. For this reason, coordinate transformation was applied by replacing n with $1/n$ for the horizontal ordinate. Afterwards, the calculation process was further modified by randomly choosing sufficient observation regions for each point uniformly distributed on the new horizontal ordinate with a certain interval. It is found that the computational precision is high enough with 50 times of randomly choosing for each point and an interval equal or less than 0.1 between two points on the horizontal ordinate. The final result is shown in Fig. 4d. As can be seen, all the curves are concave and go through (0,1) and (1,0) points.

Since the influences of the scale of the observation region and the statistical errors have been eliminated, this curve can be regarded as an intrinsic property of the grout vein distribution.

Finally, we propose the following expression (Eq. (5)) of a parameter $\bar{r}$ called "grout vein uniformity", to characterize the distribution of grout and soil in the sample. Its value depends on the area of the region bounded by the line of "$x=1$", "$y=1$" and the variance curve in Fig. 4d. A larger value represents a more homogeneous medium of the sample as a soil–grout mixture. Since the variance curve is always concave, the value of $\bar{r}$ is always greater than 0.5 and less than 1. The values of $\bar{r}$ for the samples in Fig. 4a are 0.76, 0.77, 0.94 and 0.95, respectively.

$$\bar{r} = 1 - \int_0^1 \bar{S} \cdot dx. \tag{5}$$

It should be noted that in order to make it comparable for all the samples, a same normalization factor should be used, which means the grout proportions in all the samples are the same by default. However, in a practical grouting work, samples from different regions of the formation have

different grout proportions. In this case, $\bar{r}$ with a value less than 0.5 may be defined at a scale of engineering interest.

3.2 Relation Between $\bar{r}$ and Compressive Strength of Grouted Soil

A fundamental feature of a grouted soil sample is that its strength decreases as the grout vein uniformity increases (Fig. 5a). This is because that the mechanical property of the
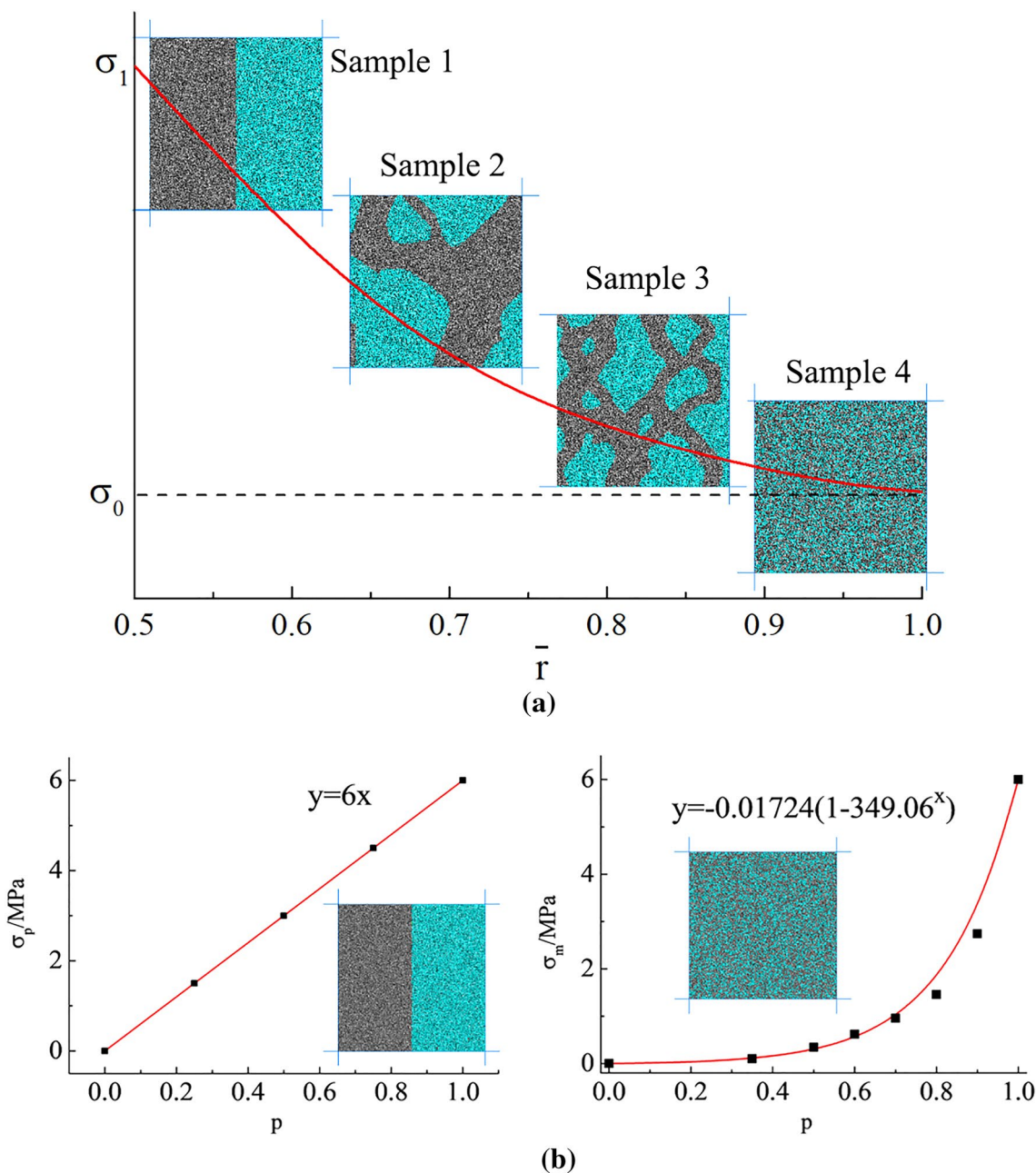

(a)

(b)

Fig. 5 Correlation between the mechanical strength and the grout parameters such as grout vein uniformity and grout proportion (**a** a general relation between the strength of grouted soil and the grout vein uniformity; **b** functional relations between the UCS and grout proportion according to regression analysis.)

sample mainly depends on the grout vein skeleton, and the strength of grout vein depends on the weakest part. Higher grout vein uniformity means a more scattered distribution of the grout vein with a larger number of branches. When the sample is loaded, failure occurs on these branches progressively, usually from the thinnest ones. Therefore, its overall strength is lower than a sample with a more concentrated grout vein, which has a more brittle property with a much lower strength after the peak.

To further investigate the relation between the compressive strength and $\bar{r}$, the two extreme cases in Fig. 5a of grout vein distribution are considered here, which corresponds to the maximum and minimum value of the compressive strength. In sample 1, the compressive strength of the sample is approximately equal to the strength of the left part, as the contribution of the soil can be neglected. Sample 4 represents an ideal state when $\bar{r}$ is approaching 1 and the grout veins are the most uniformly distributed. (Note that this state is different from a completely homogeneous sample of cement soil: the former still has a mesostructure of grout vein, which means the soil particles were excluded from the cementation process of the grout suspension when it started hardening.) For both the cases of samples 1 and 4, the influence from the morphological characteristics of grout vein is eliminated, as the grout vein has only one definite distribution (while for the other cases the distributions of grout vein can be various under the same value of $\bar{r}$, so that the strength of the samples also varies). Therefore, the compressive strength of the sample only depends on the grout proportion. Based on the PFC model, the UCS of the samples with different grout proportions was calculated, and a functional relation was obtained by regression analysis (Fig. 5b). The functional types are linear and exponential for sample 1 and 4, respectively.

It should be noted that the precision of the numerical model is limited by the amount of the particles and their radius. It is impracticable to build a sample with a grout vein structure arbitrarily thin and a value of $\bar{r}$ infinitely close to 1. In this study, grouted soil samples with $\bar{r}$ equal or greater than 0.95 were used to approximately represent the completely uniform state. A preliminary computation showed that the convergence is sufficient when $\bar{r}$ is greater than 0.95, and the relative deviation is less than 5% when using different grout vein distributions with the same $\bar{r}$. Finally, an average value of five samples with the same $\bar{r}$ and different grout vein distributions for each point were used for the regression analysis.

3.3 The Influence of Anisotropy of Grout Vein

Another factor which has an important bearing on the strength of the sample is the anisotropy of grout vein. When $\bar{r}$ is small, the anisotropy becomes obvious and the strength

of a sample varies a lot in different directions, as shown in Fig. 5a. For sample 4, $\bar{r}$ is close to 1 and it is completely isotropic. The strength is the same in all directions. In contrast, soil and grout are completely separated in sample 1. The strength in the vertical direction is approximately equal to pure grout, while in horizontal direction it is approximately equal to pure soil. For samples 2 and 3, the anisotropic behavior is between these two extreme cases. Figure 6a shows the failure regions when loaded vertically and horizontally. The elastic modulus, peak strength and failure regions are all different in these two cases.

It should be noted that the anisotropy is not necessarily related to $\bar{r}$. As shown in Fig. 6b, $\bar{r}$ decreases from left to right, while the isotropy remains unchanged. In other words, the uniaxial compressive strength increases from left to right, but the ratios of the strength in vertical and horizontal direction are the same. Therefore, the mechanical behavior of grout vein cannot be described only by $\bar{r}$, and another parameter representing the anisotropy is needed.

In this study, the anisotropic factor is defined with the following equations: first, the variances of grout proportion in the observation regions as shown in Fig. 6c are calculated (Eq. (6)):

$$S_{nx} = \frac{\sum_{i=1}^{n} (p_i - p)^2}{n}, \quad S_{ny} = \frac{\sum_{i=1}^{n} (p_i - p)^2}{n}. \tag{6}$$

The limit value of the variance is obtained when n is approaching infinity.

$$r_x = \lim_{n \to \infty} S_{nx}, \quad r_y = \lim_{n \to \infty} S_{ny}. \tag{7}$$

Finally, the anisotropic factor k is defined as the ratio of the above two values:

$$k_x = r_x/r_y, \quad k_y = r_y/r_x. \tag{8}$$

It is found that the minimum value of r_x and r_y is zero, when the grout vein is uniformly distributed in the vertical or horizontal direction (as in sample 1 of Fig. 5a). Therefore, k ranges from zero to infinite. Additionally, when $\bar{r}$ is approaching 1, the grout vein becomes uniformly distributed, and k becomes 1.

3.4 Establishment of the Formula for Estimating the Strength of Grouted Soil

Based on the above analysis, it is concluded that the strength of grouted soil σ can be regarded a function of grout proportion p, grout vein uniformity $\bar{r}$, anisotropic factor k, and the intrinsic properties of the grout and soil. It increases with an increase of p and decrease of $\bar{r}$. The maximum value of σ is approximately equal to a pure grout sample with the same grout volume. Therefore, the strength of grouted soil σ with

Fig. 6 Illustration on the influence of anisotropy of grout vein and the calculation procedure (**a** failure regions of a grouted soil sample when loaded in different directions; **b** grouted soil samples with different grout vein uniformity and the same isotropy; **c** the calculation procedure for the anisotropic factor.)

(a)

(b)

(c)
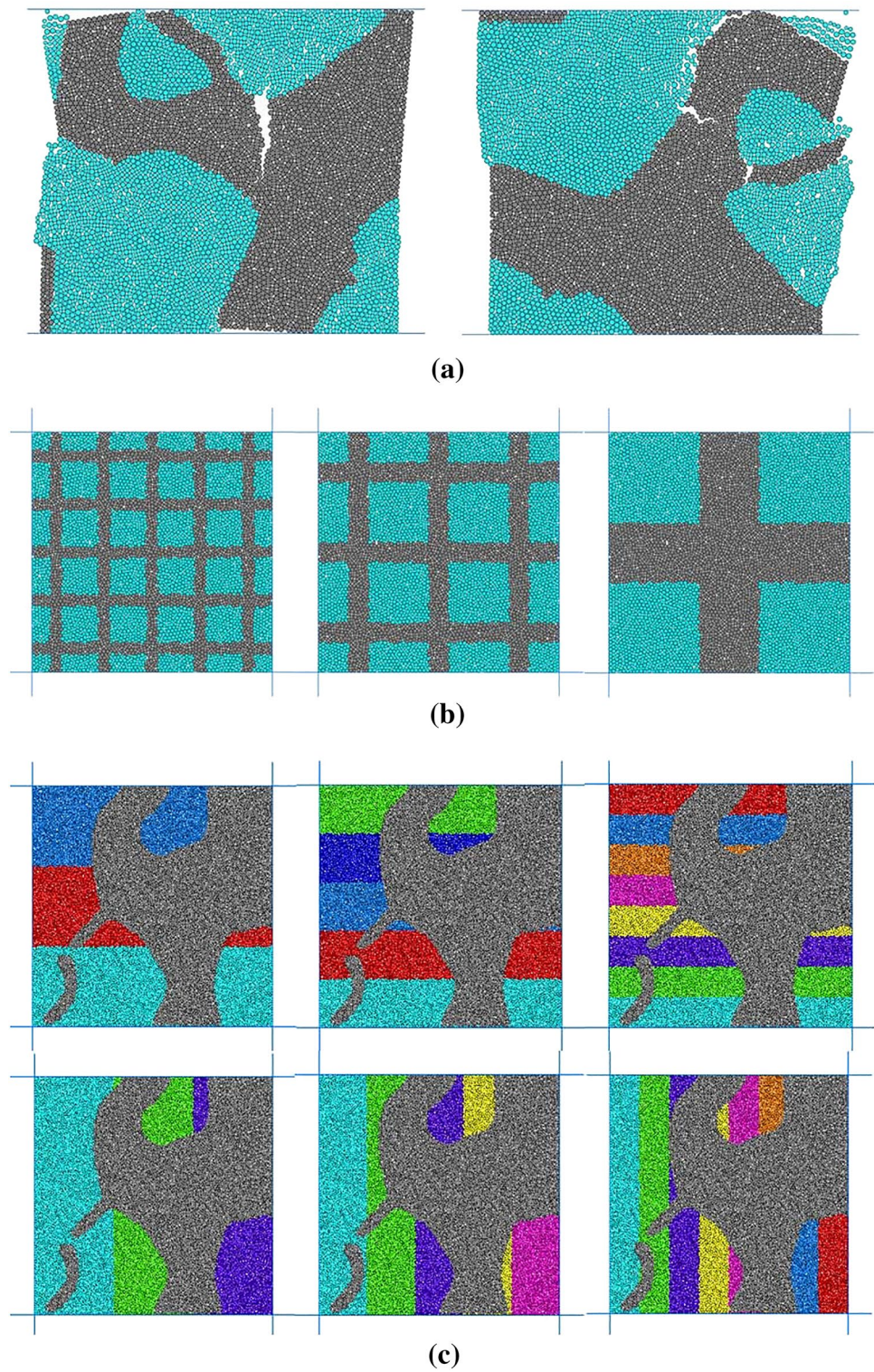
any grout vein distributions can be expressed as the strength of pure grout σ_p times a reduction factor which depends on the morphology of grout vein:

$$\sigma = \sigma_p \cdot a^{f(r,k)} \qquad (9)$$

The reduction factor is composed of a parameter a and an exponential term. Its expression can be determined according to the following boundary rules:

(i) the reduction factor ranges from 0 to 1.

(ii) $\bar{r}$ is approaching 1 (note that when $\bar{r}$ is approaching 1, k will also be approaching 1 automatically), and the grout vein distribution becomes completely uniform and σ equals σ_m.

(iii) k is approaching 0 or infinity, grout and soil completely separate from each other (as in sample 1 of Fig. 5a), and σ equals 0 or σ_p, respectively.

Therefore, Eq. (9) can be further modified into the following form:

$$\sigma = \sigma_p \cdot \left(\frac{\sigma_m}{\sigma_p}\right)^{(\bar{r} \cdot k)^A}. \tag{10}$$

The value of σ_m and σ_p under any grout proportion is determined by the regression function in Fig. 5b. It should be noted that although these functions are derived from the results of the two-dimensional PFC model, they can also be determined by any other methods such as laboratory tests and theoretical analysis and under three-dimensions. Therefore, there is only one parameter A in the equation which is unknown.

The least-square method was used to determine the value of A, based on a predicted result from Eq. (10) and a measured result from numerical uniaxial compressive tests on 70 grouted soil samples in vertical and horizontal directions. During the numerical test, some data were deleted because the anisotropy was too high and the strength was too small to be measured. Besides, the grout proportion p, grout uniformity $\bar{r}$ and anisotropic factor k of each sample were calculated, and σ_p and σ_m were determined according to their relation with grout proportion p in Fig. 5b. Since the relation between σ_m and grout proportion in Fig. 5b was derived using the samples with $\bar{r}$ around 0.95 to approximately

substitute the completely uniform state, the value of $\bar{r}$ for all the samples here was recalculated by timing a coefficient:

$$\bar{r}_a = \bar{r}/0.95. \tag{11}$$

Finally, 158 data points were used for the back calibration on A, and a value of 0.828 was obtained, with a relation of $y = 0.93 \times$ for the measured and predicted results and a correlation coefficient square of 0.90 (Fig. 7a). Additionally, the relation between $\bar{r}$ and k was also obtained (Fig. 7b). A logarithmic coordinate with a base number of 2 is adopted for y axis so that the coordinate is symmetric on $y = 1$. As can be seen, the fluctuation of k decreases as $\bar{r}$ increases. When r is greater than 0.9, the sample can be regarded as isotropic.

4 Evaluation on the Effect of Grouting Reinforcement on SRM

4.1 Conceptualization and Definition of Block-Skeleton Conversion Ratio

For grouted SRM, grout vein and rock block work together as the supporting skeleton (Fig. 8a). In ungrouted region, displacement of rock block can be very large during the deformation of soil matrix (block C). Although the strength of rock block is very high, it has little contribution on the overall strength of the formation. In grouted region, however, the dispersed rock blocks are jointed together by grout vein (block A and B). A stronger bonding between rock and grout leads to a larger contribution on the overall strength. Therefore, in order to quantify the contribution of each rock block, a parameter called "block-skeleton conversion ratio" is proposed here (represented by K), which means the ratio of the volume of a block and the equivalent volume as a
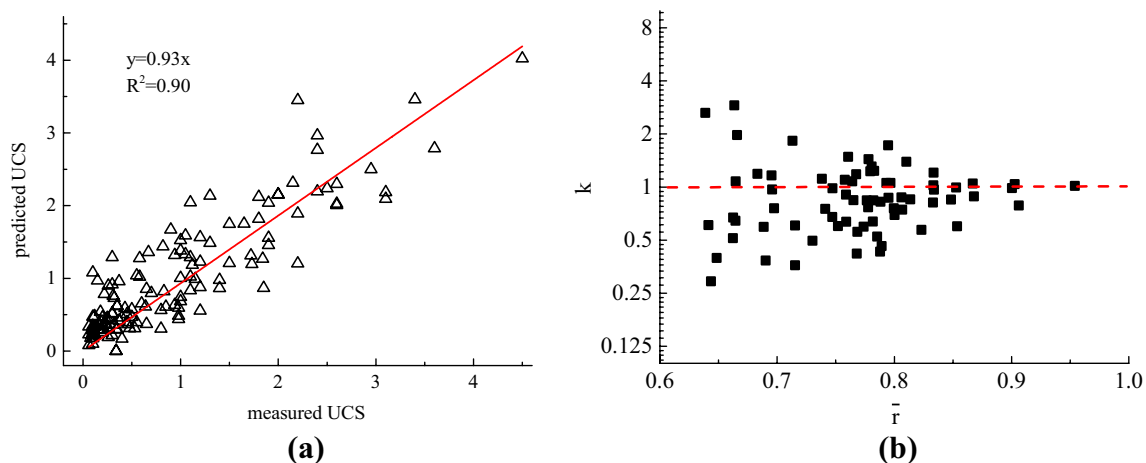

Fig. 7 Back calibration results of the UCS of grouted soil and the relation between k and $\bar{r}$

Fig. 8 Conceptualization and definition of grout vein uniformity (**a** a typical grout-rock skeleton in grouted SRM; **b** spatial relations between rock block and grout vein; **c** influence on block-skeleton conversion ratio from spatial relation between rock block and grout vein)

(a)

(b)

(c)
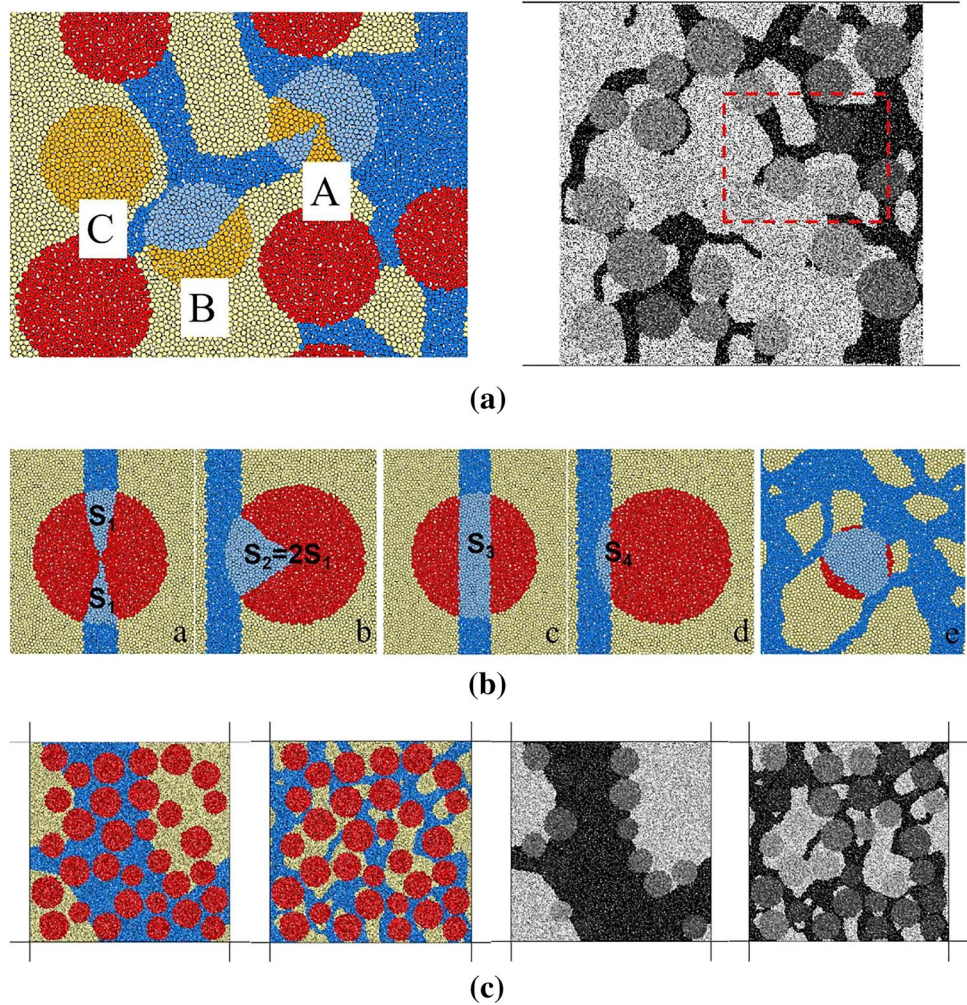
part of the grout vein so that the SRM sample has the same compressive strength.

It is obvious that K is related to the contact ratio of grout and rock. If we postulate that they are equal to each other, the "equivalent grout proportion" can be easily obtained by counting the converted volume of each block, as shown in Fig. 8a. A darker color of the blocks represents a higher conversion ratio. The strength of grouted SRM improves as the overall conversion ratio increases.

However, K is also related to spatial relation between rock block and grout vein (Fig. 8b). Sample a and Sample b show the result in which the converted volume is calculated only according to the contact ratio. Since the contact ratio is the same, the converted volumes are also assumed to be equal. Comparatively, the results in Sample c and Sample d are more reasonable, in which the converted volume of the former is larger than the latter. For a grout vein with complex morphology, one rock block may have several contact points with grout (Sample e). In this case, the bonding between rock and grout can be very strong, which leads to a high value of K, even if the overall contact area is small.

The influence of spatial relation between rock block and grout vein can be further illustrated by Fig. 8c. The grout proportions of the two samples are the same, but the latter one has a higher complexity of grout vein morphology. Most rock blocks in the first sample are either totally bonded by grout or totally unbonded, while in the other one, they are all partially bonded with several contact points. Since the rock blocks are randomly distributed and the grout proportions are the same, the overall contact ratios of the two samples are equal to each other. Therefore, the values of K of the two samples are the same if it is calculated according to the contact ratio of each rock block. But a higher value of K would be obtained if the spatial relation between each rock block and grout vein is considered.

4.2 Relation Between Skeleton Conversion Ratio and Grout Vein Uniformity

Apparently, the spatial relation between rock block and grout vein is related to grout vein uniformity. A higher uniformity leads to more contact points for each rock block. Herein,

three characteristic dimensions are defined to fully understand the influence of grout vein uniformity (Fig. 9).

Case 1 shows an extreme condition that the left and right side of the formation is completely occupied by pure grout or soil. In this case, $\bar{r}$ is assumed to be zero at the sample scale. The influence from grout vein morphology is negligible because the dimension of rock block is comparatively too small. The spatial relations between rock block and grout vein are either totally bonded or totally unbonded. Statistically, the value of K for each rock block follows a binomial distribution of 0 and 1, and the overall skeleton conversion ratio is equal to the grout proportion in the formation. In case 2, different grout vein distributions are observed at the sample scale. The spatial relations between rock block and grout vein are divided into totally bonded, totally unbonded and partially bonded (with one continuous contact surface). Grout vein morphology has a very limited effect, and the value of K in case 2 is slightly higher than case 1. In cases 3 and 4, the grout distributions are completely uniform at the scales of engineering interest. The difference becomes obvious at the mesoscale. In case 3, the spatial relations between rock block and grout vein vary from one to another, which

means grout vein morphology has an important bearing on K. However, in case 4, each rock block is sufficiently bonded with numerous contact points. The influence from grout vein morphology becomes negligible again like in case 1. Since every rock block is sufficiently bonded, K surges up to 1 as grout proportion increases.

A summary on the main features of the four cases is given in Fig. 10. The grout distributions in case 1 and 4 give the upper and lower bound on K, which are independent on grout vein morphology. The expression of K for case 4 might be obtained according to laboratory tests on artificial samples comprising fully mixed rock, grout and soil with different proportions, which is out of the scope of this study. Case 2 represents an unsatisfactory grouting result with poor coverage. The value of K is close to that of case 1. Case 3 represents a typical state which is most likely to be reached in a practical grouting work: the variance of grout proportion is almost zero at the sample scale, but the difference becomes obvious when looking at each rock block. In this case, the overall conversion ratio should be calculated by statistical methods. In the following two sections, a detailed
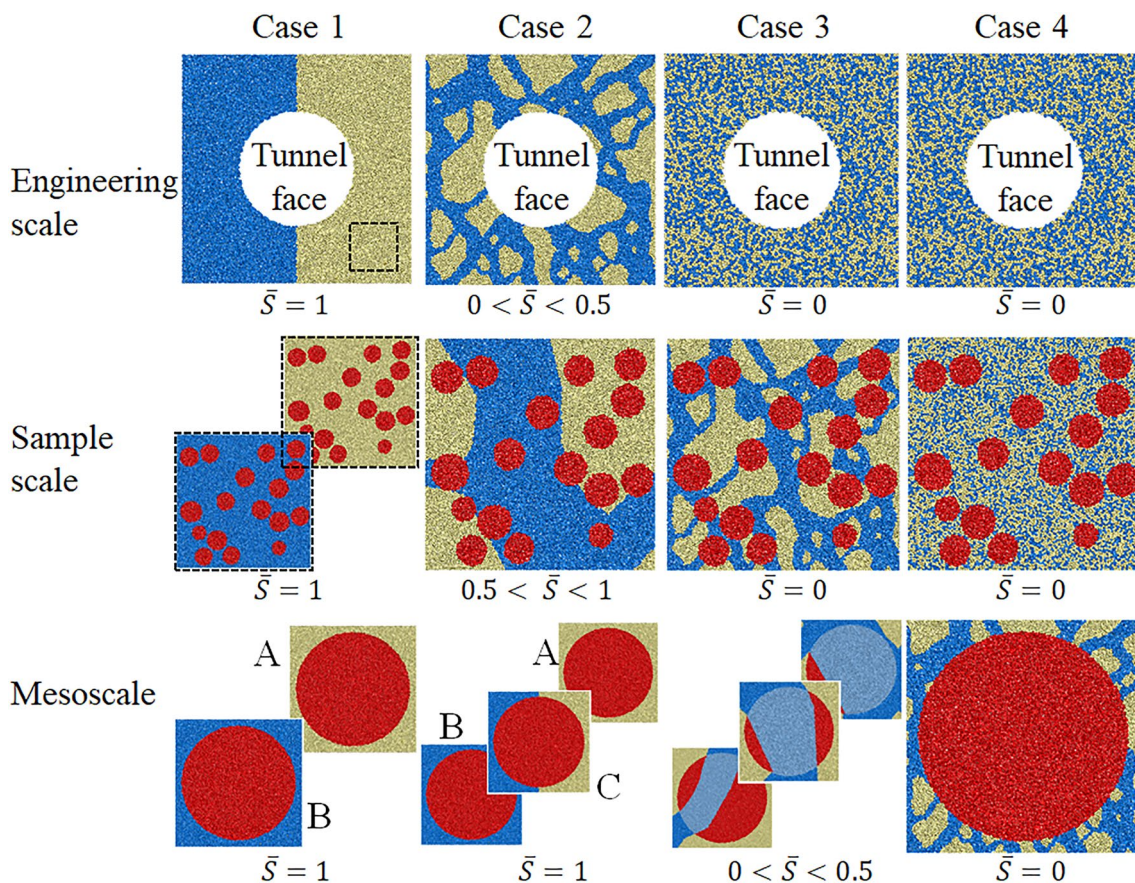

Fig. 9 Patterns of different grout vein distributions and the spatial relations between rock block and grout vein in engineering scale, sample scale and mesoscale
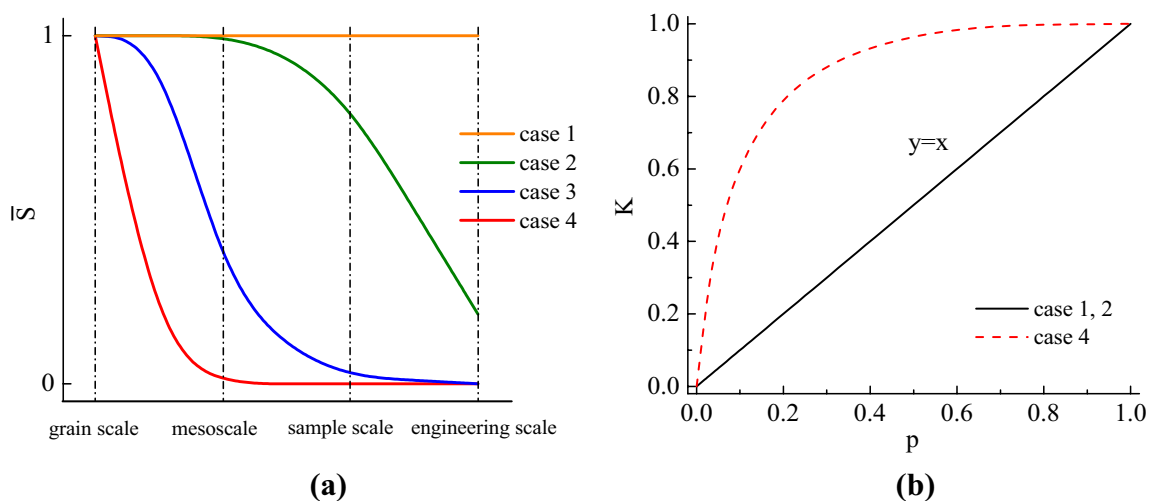
Fig. 10 The variances of the grout vein distributions on different scales and the corresponding relations between the conversion ratio and grout proportion

investigation on how to calculate the conversion ratio of case 3 is presented.

4.3 Expression of *K* as a Function of *p* for a Single Rock Block

Figure 11 shows a calculation model for determination on the expression of *K* in case 3 of Fig. 9. The grout veins are assumed to be distributed in parallel for the sake of convenience. The state in Fig. 11d is different from the others since the rock block is in contact with two grout veins, and it is excluded from the calculation. Therefore, the mathematical expectation of *K* as the rock block moves from the place in Fig. 11a–c is regarded as the minimum predicted value.

Supposing the radius of the circle is 1, the area is π and the perimeter is 2π. The arc length of AB is *l*. The contact ratio

Fig. 11 The conversion region of a single rock block with different spatial relations to grout vein and the geometric model for determination on the expression of *K*
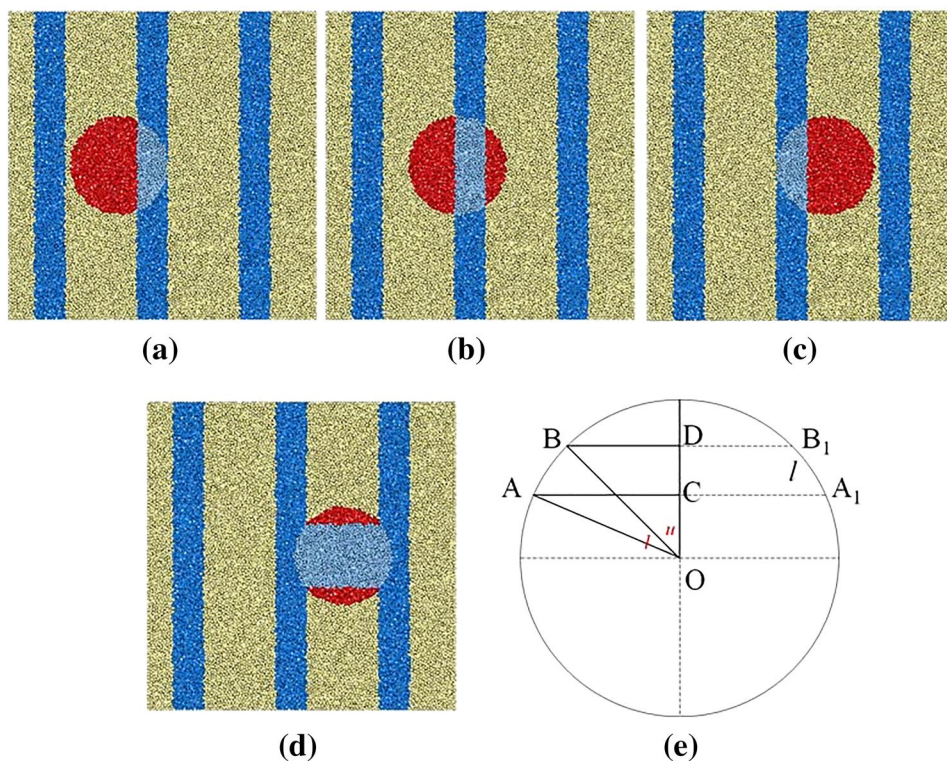
of rock and grout is l/π. The area of ABB_1A_1 is represented by s_1, which depends on the central angle l and u.

Using the geometrical relations between S_{ABCD}, S_{AOB}, S_{BOD} and S_{AOC}, and the sum to product formulas, s_1 can be represented by l and u as follows:

$$s_1 = l + \frac{1}{2}\sin 2u - \frac{1}{2}\sin 2(u + l). \tag{12}$$

The mathematical expectation of s_1 as u increases from 0 to $\pi - l$ is derived as

$$E(s_1) = l + \frac{1 - \cos 2l}{2\pi - 2l}. \tag{13}$$

The skeleton conversion ratio is derived as follows:

$$K = E(s_1)/\pi. \tag{14}$$

Since the grout vein is assumed to be uniformly distributed, the contact ratios of grout and rock for each rock block are the same and are equal to the overall grout proportion of the formation:

$$p = l/\pi. \tag{15}$$

Substituting Eqs. (13) and (15) into Eq. (14) derives the following:

$$K = p + \frac{1}{\pi^2} \cdot \frac{1 - \cos 2\pi p}{2 - 2p}. \tag{16}$$

Therefore, the function curve of Eq. (16) can be added onto Fig. 10b, as shown in Fig. 12, which represents a conservative estimation on the skeleton conversion ratio for a single rock block with the grout vein distribution of case 3 in Fig. 9.

4.4 Estimation on Compressive Strength of Grouted SRM

Another important factor for the calculation of K is rock proportion. Rock blocks may be in contact with each other when rock proportion is high. The interaction between rock block will influence the strength and deformation behavior of a sample, especially when they are bonded by grout vein. Previous studies have proved that a fundamental feature of SRM or bimrock is that the internal friction angle increases linearly with rock proportion in a range from approximately 30 to 70% (Irfan and Tang 1993; Lindquist 1994). Therefore, it is expected that the rock interaction will arise some additional strength and this influence should be included when determining the equivalent supporting skeleton and estimating the overall strength of grouted SRM.

Figure 13 shows the extreme case that the rock proportion reaches its maximum value. All rock blocks are in close contact with adjacent blocks, and the overall space in the sample is divided into many isolated voids. In this situation, the grout vein morphology disappears at the sample scale, and structures of grout vein can only be observed at a scale smaller than the voids. Therefore, the influence of grout vein reduces to a bonding effect between rock blocks. Given the grout is uniformly distributed, the bonding forces on every contact points are assumed to be equal and proportional to the grout proportion of the sample.

Herein, the strength when grout proportion reaches a hundred percent (soil matrix completely replaced by grout) is assumed to be equal to the strength of pure grout, by ignoring the strength difference between grout and rock or the interface. Afterwards, the expression of K as a function of p can be determined by comparing the strength of "sample A" with the maximum rock amount and "sample B" comprising
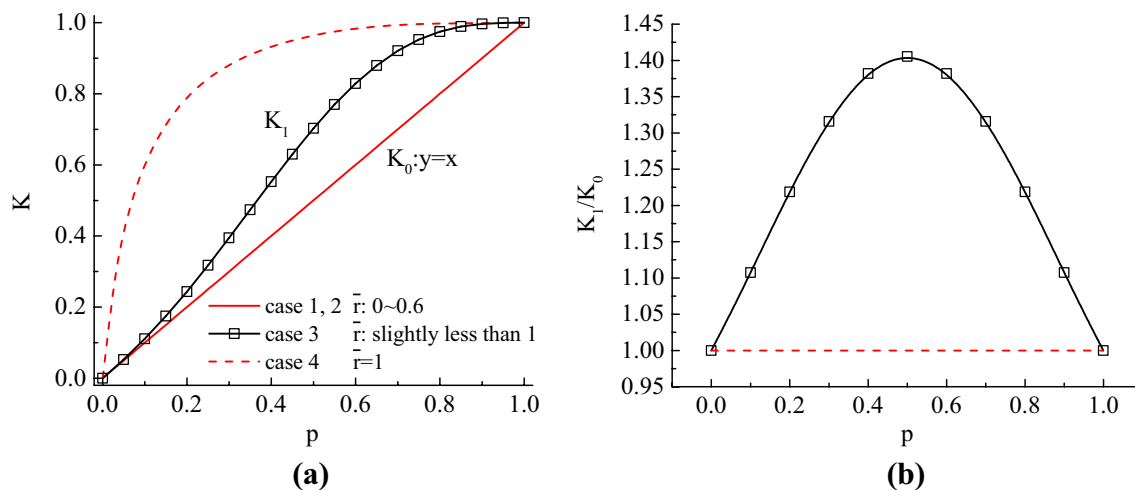

Fig. 12 The relations between the conversion ratio and grout proportion for grouted SRM containing a single rock block

Fig. 13 The equivalent model for a grout SRM sample with the maximum rock proportion
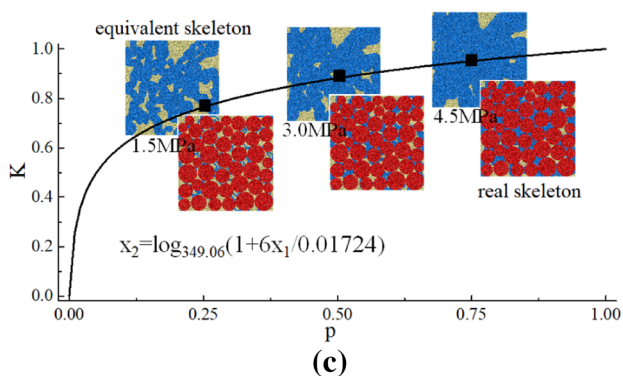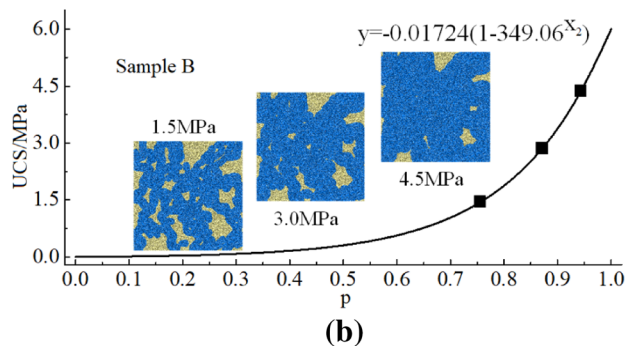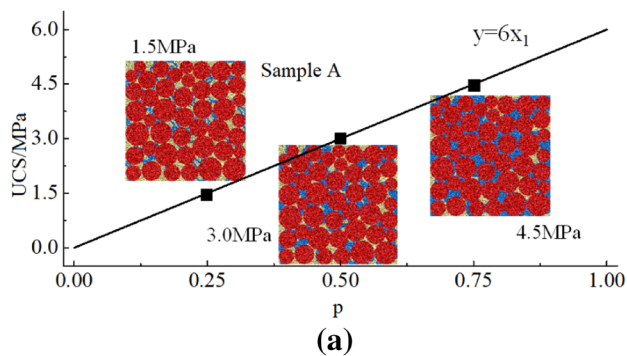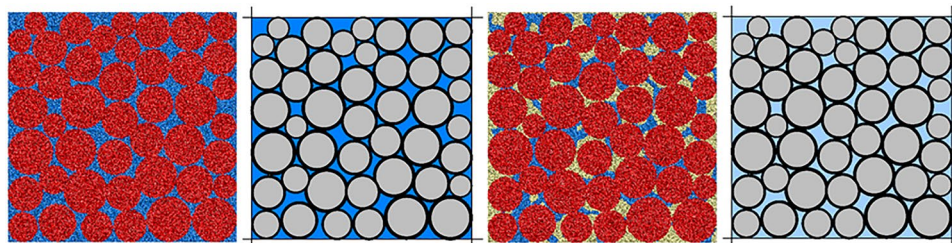

Fig. 14 The relations between the conversion ratio and grout proportion for grouted SRM with the maximum rock proportion

Fig. 15 The complete description of rock conversion ratio as a function of grout proportion and rock proportion

soil matrix and a skeleton of grout vein, as shown in Fig. 14. The strength of sample A is assumed to be proportional to grout proportion, and the strength of sample B is calculated according to the equation in Fig. 5b. K is the ratio of p_B and p_A which keeps the strength of the two samples the same.
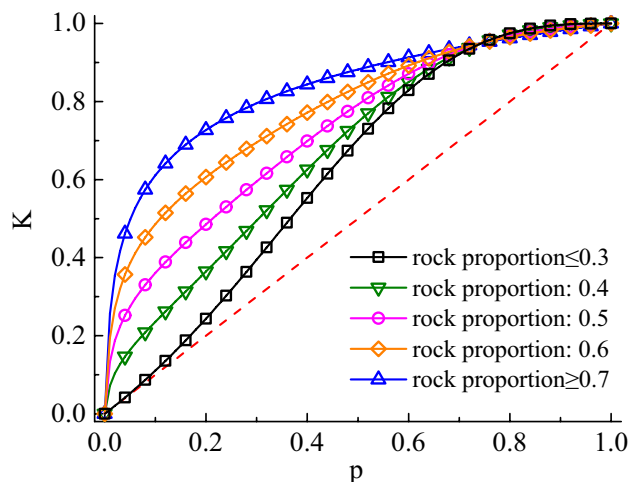
Note again all these fitting functions can be replaced by laboratory test results or derived by other available strength theories. The accuracy of the proposed formula and approach does not rely on the PFC model used in this study.

Based on the above analysis, another function curve (Fig. 14c) can be added onto Fig. 14b. Therefore, the function curves in Figs. 14c and 12a determine the upper and lower limit of the influence on the rock conversion ratio from rock interaction. Herein, this influence is assumed to be negligible when rock proportion is less than 30% and reaches the upper limit when rock proportion is greater than 70%. In between, the rock conversion ratio and rock proportion obey a linear relation. This is based on the previous research results of the relation between grout proportion and internal friction angle for ungrouted SRM (Irfan and Tang 1993; Lindquist 1994) and on the fact that increase of rock proportion causes a strength transition from grouted SRM to rock-fill with bonding. The complete description of rock conversion ratio as a function of grout proportion and rock proportion is shown in Fig. 15.

Numerical simulation of uniaxial compressive test on grouted SRM with different grout vein and rock block distributions were conducted. 35 data of UCS were obtained as the measured values. Meanwhile, the predicted values were obtained by calculating the block conversion ratio and

equivalent grout proportion according to the relations in Fig. 15. A comparison result is shown in Fig. 16. As can be seen, a well-correlated relation between the measured UCS and predicted UCS was obtained, which justifies the rationality of the proposed approach for estimating strength of grouted SRM.

5 Experimental Validation

The experimental validation is divided into two parts. The first part aims at verifying the influence of the morphological parameters (especially the grout vein uniformity $\bar{r}$) on the mechanical behavior of grouted soil. The second part aims at testifying the accuracy of the proposed approach when predicting the strength of grouted SRM with different grout and rock proportions.

5.1 Devices and Procedures

As mentioned earlier, it is extremely difficult to prepare test specimens with prefabricated grout vein structures. Additionally, the fracturing path is uncontrollable during the grouting process. Therefore, it is almost impossible to reproduce specimens with the same morphological structure of grout vein. In this study, two methods were adopted for specimen preparation, namely "independent injecting (II) method" and "direct pouring-in (DP) method", as shown in Fig. 17. A detailed description of the two methods is given below.
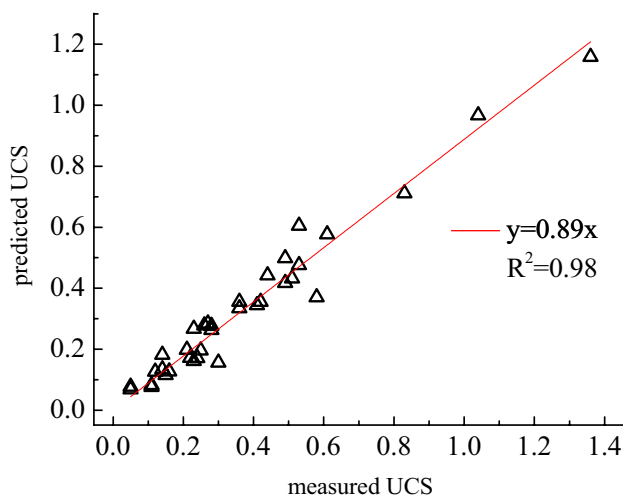

Fig. 16 Comparison between the predicted UCS and measured UCS of the grouted SRM

5.1.1 Independent Injecting Method

The procedure of the independent injecting test is in consistent with the previous work of Liu et al. (2019), which is to directly inject grout suspension into a mixture of soil–rock confined in a cylindrical rigid container with top and bottom lids. The inside diameter of the container is 10 cm and the height is 25 cm. The thickness of the cylinder wall and lids is 1 cm, which ensures that there is no deformation during grout injection. The container is filled up with soil and rock blocks in a certain ratio before it is screwed up in case of leakage when grouted. A tube is buried in the mixture and connected to the injection hole on the top of the container during the filling process. The tube is 20 cm-long with multiple holes on the side. Grout suspension is injected through the injection hole and flow out at the side-holes. Therefore, the injection process is assumed to obey the cylindrical diffusing condition. After solidification, the specimen is taken out from the container and the bottom layer of pure soil is cut off before the uniaxial compressive test is conducted.

The independent injecting keeps the integrity of the specimen compared with the large-scale grouting test, which has a big problem of obtain undisturbed specimens from the grouted SRM with coring. Besides, it ensures that the composition of the medium and grouting parameters are controllable and accessible, while for the large-scale grouting test the fluid pressure decreases in the distance, and the grouting parameters in different regions may be highly scattered. However, for independent injecting, since no deformation on the boundary is allowed during grouting, the grout vein can make a room for itself only by squeezing the pore voids in the matrix. To ensure that sufficient grout can be injected to construct an effective supporting skeleton, the initial porosity of the matrix should be rather high. Therefore, the infilled soil was in a rather loose state, which may cause a different fracturing mechanism compared to that in the consolidated soil. Additionally, the fracturing path might be different from a real grouting work, due to the cylindrical diffusing condition confined in the small space of the container. A more detailed description of the procedures can be found in the work of Liu et al. (2019).

5.1.2 Direct Pouring-In Method

The direct pouring-in method is much simpler in the way of grout vein generation. Soil blocks are used as the infilling medium instead of granular soil. The container is a cubic with a length of 10 cm. The reason for not using the same container shape of the injection method is because gravity effect on cement particles in the grout suspension would be significant in this method if the ratio between the height and width is high, which may influence the uniformity of

(a)

(b)
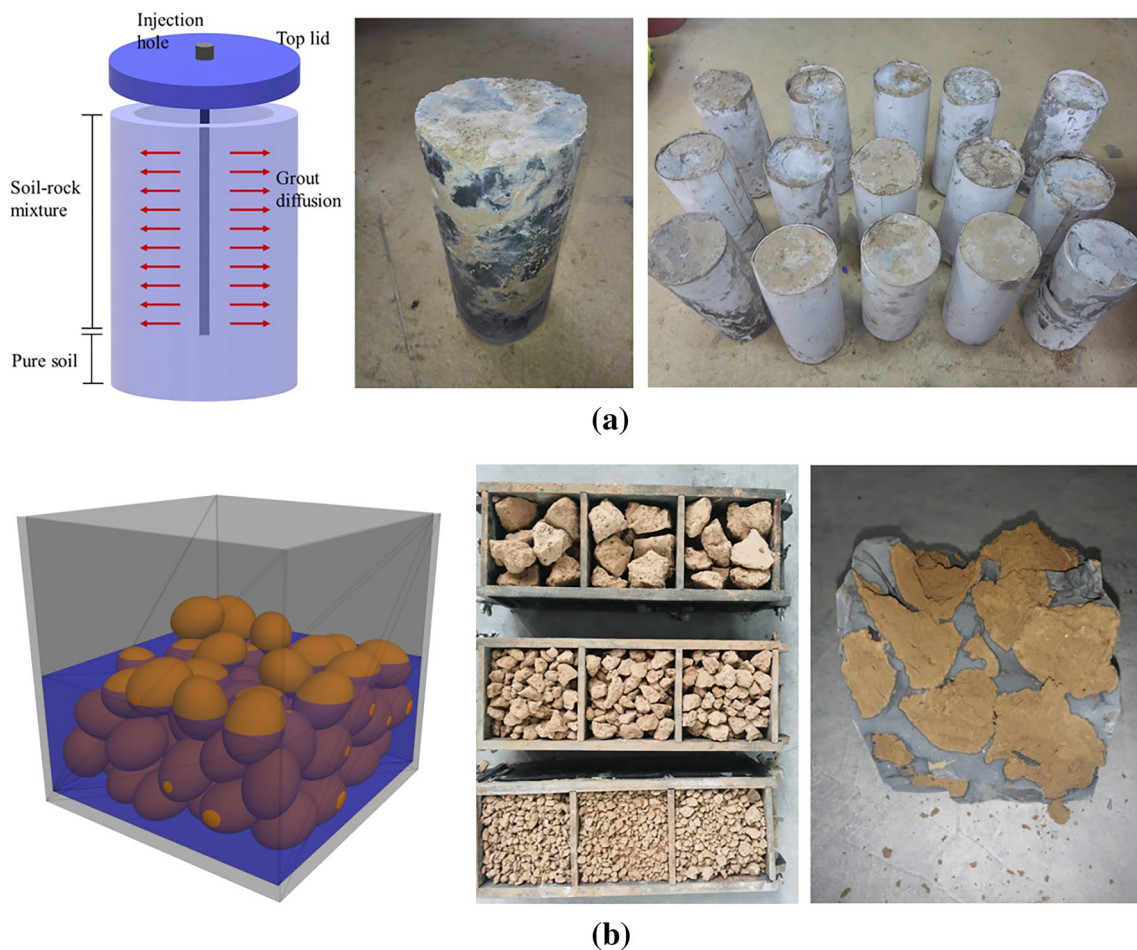
Fig. 17 Preparation for test specimens with I-I method and D-P method

the concentration of grout suspension and the strength after solidified.

Grout suspension is poured into the container after being filled with soil and rock blocks. In this way, the fracturing process is replaced by the direct filling of grout, and the soil is pre-consolidated instead of being compacted by grouting pressure. The morphological structure of grout vein is predetermined as the contour of the connected pore voids between the soil and rock blocks. Therefore, the grout vein is more uniformly distributed in the matrix compared with the injecting method, which may cause over-concentrated grout bulks in some local regions due to excessive compaction on the soil matrix. However, this method suffers from the problem of the artificial grout vein structure which might be different from that in a real grouting work.

5.2 Properties of Selected Material

SRM specimen was prepared using soil and rock blocks at different ratio. The following properties of the soil were obtained with laboratory tests: unit weight of volume $\gamma_s = 23$ kN/m^3, liquid limit $w_1 = 29$, plasticity index $I_p = 10$. The soil was oven-dried at 120 °C for one day before being used for preparing the mixture. The rock block has a roughly round shape with a unit weight (represented by γ_r) of 29 kN/m^3. After preparation, the soil and rock blocks are sufficiently mixed in the container waiting to be injected or filled with grout suspension. The shape of rock blocks was controlled with the long axis of 4–5 cm and the short axis of 2.5–3.5 cm. The grain size distribution curve of the soil, as determined by ASTM D 422-63, is shown in Fig. 18.

Grout suspension is composed of Portland ordinary cement and water with a mass ratio of 1:1, which can be regarded as Newton fluid when flowing. The groutability number N (characterized by the ratio between grain diameter of soil D_{15} and the cement particles d_{85}) is 7.5, which means the suspension can hardly penetrate into the voids of soil matrix during the injection or pour-in process.

Fig. 18 Grain size distribution curve of the soil

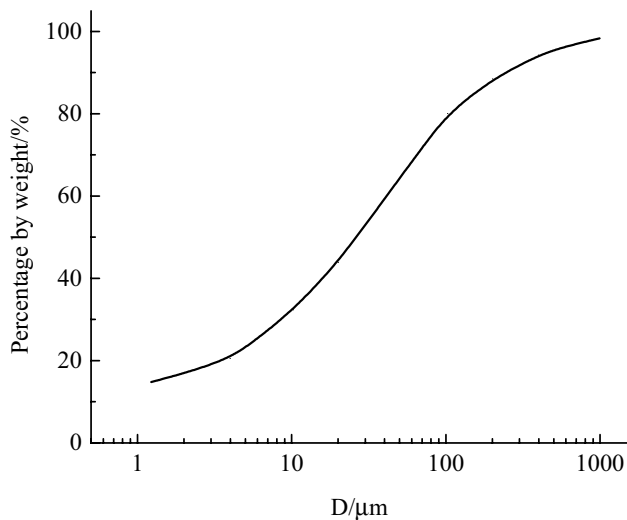## 5.3 Experimental Series

A parametric analysis was performed by varying the block size, water–cement ratio of the grout, and the proportion of grout, soil and rock in the specimen, in order to demonstrate the effect of the block size and its distribution on the heterogeneity of the specimen, and to investigate the correlation between the composition and the mechanical behavior of grouted SRM. However, it was found that the ratio between these parameters can hardly be adjusted in an arbitrary way when using the D-P method. Since all the rock and soil blocks have to be in contact with each other, the upper and lower limits of the volume proportion of the blocks are quite limited while the size and shape of the blocks stay the same. The same problem also occurs when using the I-I method: A larger amount of grout to be injected needs more pore voids for squeezing, which means the initial state of soil matrix is very loose and does not satisfy fracturing grouting. On the other hand, an insufficient amount of grout cannot generate an effective supporting skeleton covering the entire region of

soil matrix. In a word, both excessively higher or lower grout proportion to be injected will cause an unrealistic diffusion process or grout vein skeleton, which is different from the one dominated by the typical fracturing mechanism.

After several tries in a preliminary test, two block proportions (0.4 and 0.6) were finally adopted for making the specimen. In other words, the volumetric ratio between grout suspension and the sum of soil and rock blocks was either 0.4 or 0.6, while the ratio between soil and rock for each series ranges from 0 (grouted soil) to 1 (welded bimrock). It should be noted that, although the variation of grout proportion in the experiment cannot cover the whole range from 0 to 1, it is in accordance with a grout operation of the real world for which the grout take varies in a certain range per injection hole and is in proportion with the diffusion distance.

The experiment series performed using different material parameters are summarized in Table 2.

After preparation, specimens are cured for 28 days at the 100% relative humidity and temperature of 25 ± 5 °C before used for compression test. The uniaxial compressive test is carried out in accordance with ISRM (1981) at a constant loading rate of 0.05 mm/s. Each time the specimen is loaded until the axial stress falls below 70% of the peak stress.

5.4 Comparison of Results with Theoretical Values and Discussion

The influence of the grout vein uniformity on the mechanical behavior of grouted soil was investigated by varying the size of the soil and rock blocks in the specimen. It was found that the dispersion of the UCS is in a positive correlation with the block size. The grout vein can be regarded as uniformly distributed when block size is smaller than 1 cm. The correlations between the UCS and grout proportion for all the parameter combinations are summarized in Fig. 19 by normalizing all the values using the UCS of one specimen with the same size made of pure grout. Each point was calculated by averaging at least 3 data from the uniaxial compressive test. As can be seen, the UCS is in a positive correlation with

Table 2 Experiment series and the material parameters

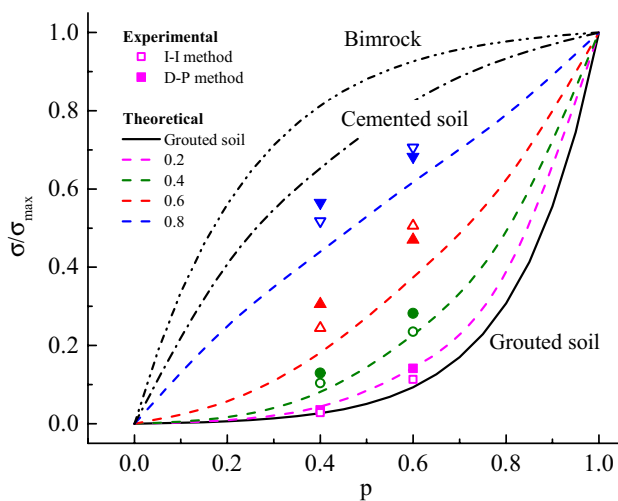|		D-P method			I-I method			Cemented soil
Grout proportion		0.4/0.6			0.4/0.6			0/0.2/0.4/0.6/0.8/1
Rock-soil ratio		0/0.2/0.4/0.6/0.8/1			0/0.2/0.4/0.6/0.8/1			–
	Grain size/cm		Water-cement ratio	Grain size/cm		Water-cement ratio	Grain size/cm		Water-cement ratio
	Soil	Rock		Soil	Rock		Soil	Rock	
Properties of soil, rock and grout	0.7	0.7	1.2	Matrix	0.7	0.8/1/1.2	Matrix	–	0.8/1/1.2
	1	1	1/1.2	Matrix	1	0.8/1/1.2			
	3	3	0.8/1/1.2	Matrix	3	0.8/1/1.2			

Fig. 19 Correlation between the UCS and grout proportion for Grouted SRM with different rock-soil ratio (The solid line and the dashed lines are obtained according to the proposed theoretical model, which represent pure grouted soil and grouted SRM with a rock-soil ratio of 0.2, 0.4, 0.6 and 0.8, respectively; The dash-dotted line represents cemented soil which is obtained by fitting the test data of this study; the dash-dot-dotted line represents bimrock according to the study of Sonmez et al. (2006))

the rock-soil ratio, and the contribution from rock block is more significant for a specimen with a low grout proportion or a high rock proportion. This is in consistent with the analysis of Sect. 4. The test data basically agree with the predicted values from the theoretical model, especially in the lower end of the range of rock-soil ratio. The possible reasons for the error lie in two following aspects:

First, the morphology of the skeletons was affected by the experimental procedures and may be different from the actual situation of the in-site grout operation. For example, the fracturing path is sometimes uncontrollable when using I-I method. Grout vein was likely to be confined around the injection tube and can hardly form an entire supporting skeleton when the grout amount is small. Second, the theoretical model proposed in this study may overestimate the strength when the rock-soil ratio is higher than 0.9, owing to the assumption that all rock blocks will be completely bonded by grout vein as long as the grout proportion is in a high level (regardless of the absolute amount of grout vein). In fact, the flow pattern during grouting and the mechanical property of the medium after grout solidification changes significantly as the rock-soil ratio increases to a high level, which may contradict the basic assumptions of grout vein structure (Liu et al. 2019). This deficiency can be offset by considering the strength models of bimrock as the upper bound and excluding the unrealistic curves with high rock-soil ratio (Sonmez et al. 2006). However, those correlations are not incorporated into the current model in order to keep the concision of its formula.

Additionally, it is found that the normalized UCS increases in a linear fashion over grout proportion at a rock-soil ratio between 0.6 and 0.8. That is to say, for a grout take equal to half the volume of the stratum, the expected mechanical strength after grout reinforcement is almost 50% of that of pure solidified grout. However, when the rock-soil ratio is lower than 0.2, the strength improvement of the stratum can only reach 10% of the grout. In a grouting work of the real world, the expected grout take in the stratum can be estimated on the basis of the groutable volume of the voids in the medium and the compressibility of the soil matrix. Afterwards, the improvement of the mechanical property of the stratum can be quickly assessed according to the above correlation as a general rule.

Practically, a stratum with only a few rock blocks is assumed as the worst situation since the scattered blocks severely weaken the compatibility of deformation of the original medium and the homogeneity of the supporting skeleton after grouting reinforcement (Liu et al. 2019). In this case, a normal grouting work can hardly achieve a satisfied reinforcement effect. In contrast, a stratum of pure soil is free from the influence of the weak interface between rock and soil on the fracturing path during grouting, while the criterion of fracture initiation for SRM and pure soil is different from each other. Therefore, an alternative method such as compaction and permeation grouting will likely be preferred according to the specific engineering projects and the excavation and supporting technics.

Another interesting finding is the discrepancy between grouted and cemented soil and the similarity between cemented soil and bimrock. At low grout proportion, the UCS of cemented soil is much higher than grouted soil, and even higher than grouted SRM with a high rock proportion. This further demonstrates the influence of heterogeneity of grout vein structure on the macro mechanical behavior of the grouted medium. Even though the grouted soil was generated in a rather uniform way in this study (by pouring grout suspension into the container filled with small soil blocks), the heterogeneity of grout vein structure still exists in a microscale, which leads to a fundamental difference comparing with the micro-structure of cemented soil, in which cement and soil particles are sufficiently mixed and bonded during the cement hydration reaction. On the other hand, the cohesive force on the grout–rock interface is assumed to be quite close to the cohesion in the interior of grouted soil. The weakness of the interface is not that significant and is partially compensated by the high strength of grout and rock. Therefore, these two curves have a similar form, while the overall strength of bimrock is a little bit higher.

6 Conclusions

In this study, a preliminary theoretical model and an empirical formula was developed for predicting the overall strength of grouted SRM according to the actual morphological structure of grout-rock skeleton and its heterogeneity. The morphology of grout vein and the structural effects of the supporting skeleton in a specimen are characterized by two new parameters: grout vein uniformity $\bar{r}$, and anisotropic factor k. The strength of the supporting skeleton decreases as the grout vein uniformity increases since the branches become thinner and easier to be crushed. Meanwhile, the mechanical property of the specimen becomes more isotropic.

The strength of a grouted soil specimen can be regarded as the strength of pure grout with a reduction factor. In this study, the reduction factor was supposed to be an exponential function of $\bar{r}$ and k, and the expression was determined by a series of boundary rules. The developed formula comprises mechanical and morphological parameters with clear definition which can be easily measured with laboratory tests, and one empirical parameter A, which was determined by the least-square method in this study.

Rock blocks can make a contribution to the macroscopic strength only if they are bonded by grout vein. This contribution can be quantified by the new parameter: block-skeleton conversion ratio K, which depends on the spatial relation between rock block and grout vein, bonding effect, and interaction between the blocks. In this study, the spatial relations between rock block and grout vein were comprehensively investigated by scanning the features of grout vein distribution from the engineering scale to mesoscale. Based on that, K can be estimated as a function of grout and rock proportions.

The ability of the developed approach to capture main factors of mechanical properties was verified by comparing the predicted values of the UCS of artificial SRM specimens with the measured values from the PFC simulation result, and with the laboratory test results according to the so-called I-I method and D-P method. The comparison with the numerical results shows a high level of consistency since both of them are developed on the basis of a two-dimentional condition. The discrepancy of the laboratory test is slightly larger, since the UCS result also includes the influence of the cleanliness and the roughness of the rock surface, as well as the real grouting conditions during grout vein generation.

Results show that the normalized UCS increases in a linear fashion over grout proportion at a rock-soil ratio between 0.6 and 0.8. The improvement of the mechanical property of the stratum can be quickly assessed according to the obtained correlations as a general rule. However, the theoretical model proposed in this study may overestimate the strength when the rock-soil ratio is higher than 0.9. Besides, the data could not cover the whole value range of grout proportion, owing to the restrictions of the experimental methods during grout vein generation. Therefore, it is open to improvement by further studies to better understand the bonding force as well as the structural effects and interaction between rock blocks. What is more, more researches are needed for the generalization of the proposed theoretical model into three-dimensional conditions and for the systemization of a more rigorous and robust approach in estimating and accommodating the uncertainties when applied in grouting operation guidance in the real world.

Appendix 1

See Table 3, Fig. 20.

Table 3 Calculation details of Fig. 7

No	Measured value		σ_p	σ_m	p	r_y	r_x	$\bar{r}$	$\bar{r}_a$	Predicted value	
	σ_y	σ_x								σ_y	σ_x
1	0.980	0.980	2.974	0.297	0.496	0.679	0.631	0.665	0.697	0.485	0.595
2	0.120	0.120	2.830	0.256	0.472	0.929	0.833	0.738	0.774	0.337	0.478
3	1.400	0.200	3.249	0.393	0.541	0.582	0.917	0.759	0.796	0.978	0.255
4	2.200	0.400	3.335	0.429	0.556	0.467	0.893	0.785	0.823	1.202	0.169
5	1.100	–	3.139	0.352	0.523	0.399	0.951	0.768	0.805	1.289	0.073
6	1.650	1.000	4.472	1.338	0.745	0.769	0.880	0.806	0.845	1.749	1.382
7	0.060	0.100	1.917	0.095	0.320	0.936	0.717	0.781	0.818	0.080	0.248
8	4.500	2.200	5.504	3.693	0.917	0.744	0.947	0.906	0.950	4.024	3.450
9	0.980	–	2.550	0.190	0.425	0.671	0.874	0.778	0.815	0.439	0.167
10	1.800	0.350	3.978	0.819	0.663	0.560	0.944	0.689	0.722	1.817	0.621
11	1.000	0.900	4.484	1.353	0.747	0.942	0.893	0.797	0.835	1.525	1.670
12	0.670	0.060	3.294	0.412	0.549	0.479	0.934	0.662	0.694	1.360	0.228
13	2.600	0.100	3.675	0.605	0.613	0.275	0.943	0.644	0.675	2.298	0.099
14	1.200	2.950	4.775	1.804	0.796	0.898	0.646	0.810	0.849	1.563	2.500

Table 3 (continued)

No	Measured value		σ_p	σ_m	p	r_y	r_x	$\bar{r}$	$\bar{r}_a$	Predicted value	
	σ_y	σ_x								σ_y	σ_x
15	1.730	0.800	3.391	0.455	0.565	0.500	0.828	0.715	0.750	1.194	0.307
16	2.000	0.320	4.383	1.225	0.731	0.523	0.915	0.823	0.863	2.154	0.730
17	1.100	1.500	3.776	0.670	0.629	0.775	0.653	0.683	0.716	0.833	1.209
18	0.260	0.240	3.263	0.399	0.544	0.689	0.909	0.697	0.731	0.899	0.424
19	0.100	1.900	3.568	0.543	0.595	0.949	0.518	0.713	0.748	0.311	1.456
20	2.500	0.350	3.893	0.753	0.649	0.368	0.930	0.648	0.680	2.238	0.297
21	–	0.120	1.596	0.065	0.266	0.781	0.527	0.761	0.797	0.040	0.234
22	2.400	0.350	4.530	1.416	0.755	0.400	0.931	0.788	0.826	2.765	0.616
23	0.940	–	1.826	0.085	0.304	0.351	0.917	0.690	0.724	0.633	0.010
24	2.400	0.180	4.175	0.997	0.696	0.474	0.954	0.730	0.765	2.196	0.537
25	1.720	1.900	4.309	1.139	0.718	0.792	0.722	0.758	0.794	1.313	1.557
26	–	0.100	2.915	0.279	0.486	0.827	0.419	0.666	0.698	0.137	1.081
27	1.500	0.300	4.384	1.226	0.731	0.754	0.895	0.765	0.802	1.746	1.289
28	3.100	1.850	4.365	1.203	0.728	0.495	0.825	0.752	0.788	2.183	0.867
29	1.200	0.650	3.614	0.569	0.602	0.527	0.828	0.782	0.819	1.228	0.371
30	1.300	1.000	4.187	1.009	0.698	0.777	0.943	0.788	0.826	1.487	1.005
31	1.900	0.580	4.365	1.203	0.728	0.641	0.947	0.747	0.783	2.037	1.020
32	0.100	–	1.498	0.057	0.250	0.451	0.978	0.789	0.827	0.344	0.008
33	0.370	2.200	4.322	1.153	0.720	0.976	0.679	0.778	0.815	0.957	1.891
34	1.000	2.600	4.270	1.096	0.712	0.926	0.538	0.795	0.833	0.682	2.026
35	0.260	2.600	3.628	0.577	0.605	0.913	0.347	0.639	0.670	0.192	2.007
36	0.820	0.430	3.704	0.623	0.617	0.605	0.903	0.663	0.694	1.437	0.591
37	0.320	0.120	2.580	0.197	0.430	0.816	0.940	0.795	0.833	0.360	0.214
38	2.400	3.400	5.305	3.038	0.884	0.834	0.691	0.834	0.874	2.964	3.462
39	2.150	3.600	4.995	2.239	0.832	0.788	0.667	0.767	0.804	2.314	2.786
40	0.940	0.580	4.177	0.999	0.696	0.888	0.904	0.747	0.783	1.320	1.275
41	0.200	0.800	2.952	0.290	0.492	0.926	0.755	0.780	0.817	0.289	0.563
42	1.300	1.800	4.861	1.962	0.810	0.816	0.820	0.853	0.894	2.135	2.119
43	2.000	1.100	4.828	1.900	0.805	0.847	0.877	0.834	0.874	2.148	2.045
44	1.150	0.500	3.583	0.552	0.597	0.706	0.932	0.800	0.838	0.991	0.468
45	3.100	1.400	4.160	0.982	0.693	0.494	0.814	0.641	0.672	2.091	0.865
46	1.200	–	2.410	0.164	0.402	0.547	0.919	0.774	0.811	0.553	0.075
47	0.100	–	2.088	0.115	0.348	0.586	0.909	0.665	0.697	0.469	0.095
48	1.050	0.300	4.059	0.888	0.677	0.775	0.922	0.782	0.820	1.329	0.916
49	–	1.100	2.358	0.155	0.393	0.981	0.338	0.663	0.695	0.018	1.024
50	0.550	0.150	3.785	0.676	0.631	0.831	0.859	0.696	0.729	1.040	0.968
51	0.500	0.160	3.086	0.333	0.514	0.791	0.969	0.833	0.873	0.574	0.293
52	0.830	0.300	3.594	0.558	0.599	0.794	0.935	0.848	0.889	0.821	0.518
53	1.050	0.400	4.012	0.848	0.669	0.568	0.949	0.854	0.895	1.588	0.459
54	1.840	0.300	3.793	0.681	0.632	0.662	0.955	0.800	0.839	1.268	0.507
55	0.550	0.100	2.679	0.218	0.446	0.772	0.853	0.759	0.795	0.397	0.281
56	0.080	–	2.223	0.134	0.370	0.852	0.809	0.793	0.831	0.179	0.221
57	1.200	–	2.253	0.138	0.376	0.342	0.951	0.715	0.750	0.877	0.013
58	0.310	0.200	3.351	0.436	0.558	0.761	0.906	0.776	0.814	0.758	0.459
59	1.000	–	2.690	0.221	0.448	0.536	0.962	0.768	0.805	0.742	0.091
60	0.220	0.060	3.157	0.358	0.526	0.655	0.872	0.741	0.777	0.783	0.337
61	0.530	0.850	3.041	0.318	0.507	0.804	0.652	0.783	0.821	0.311	0.607
62	0.450	0.100	2.730	0.230	0.455	0.689	0.927	0.807	0.846	0.507	0.174
63	0.650	1.120	3.797	0.684	0.633	0.833	0.716	0.695	0.729	0.852	1.185
64	0.200	0.460	2.904	0.276	0.484	0.904	0.884	0.833	0.874	0.341	0.367
65	0.600	0.700	3.535	0.526	0.589	0.825	0.766	0.764	0.801	0.654	0.796
66	0.450	0.300	2.688	0.220	0.448	0.791	0.931	0.814	0.853	0.396	0.219
67	0.260	0.340	2.902	0.276	0.484	0.920	0.933	0.900	0.944	0.316	0.299
68	0.640	0.370	3.352	0.437	0.559	0.826	0.934	0.868	0.910	0.611	0.416

Table 3 (continued)

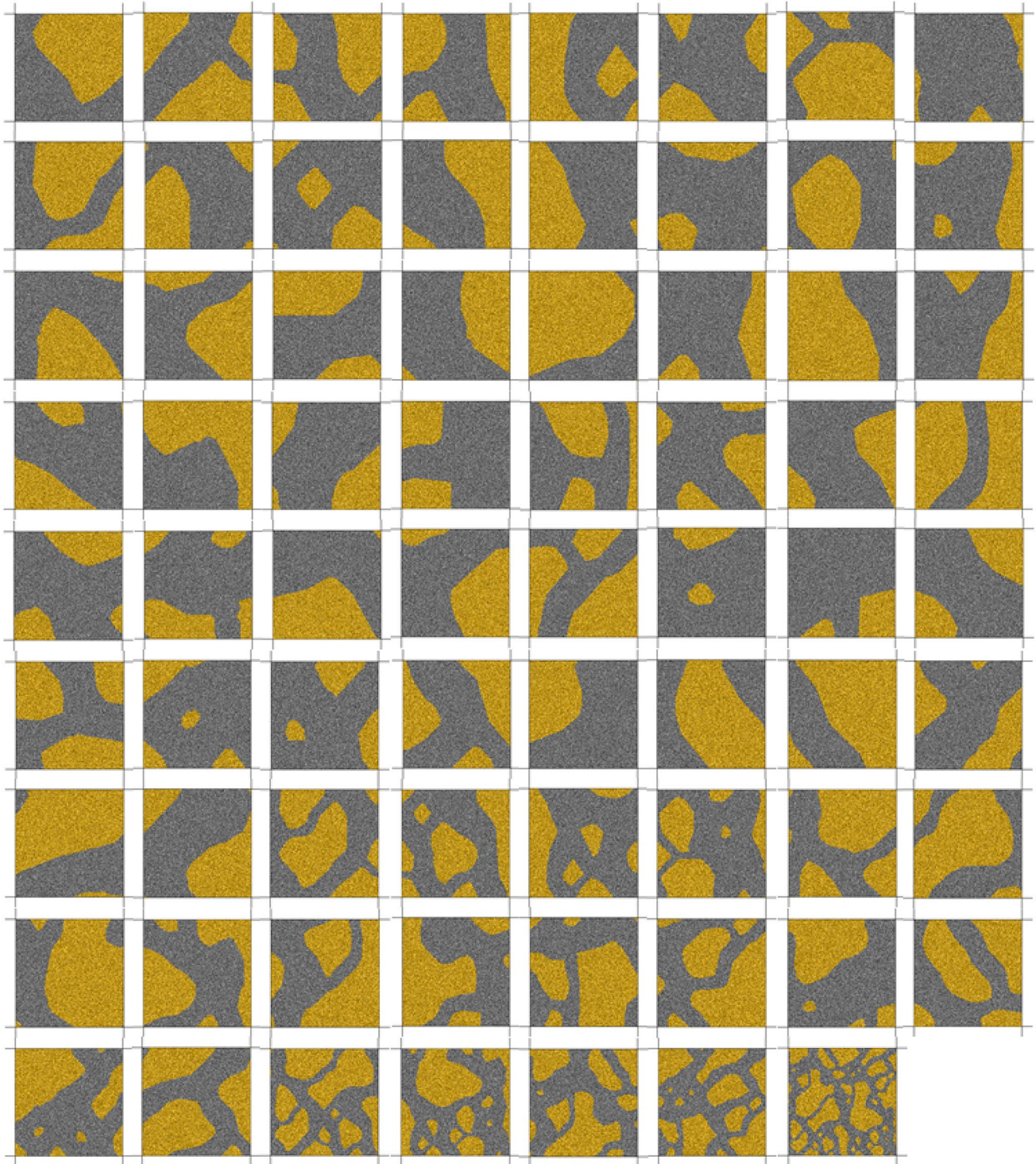| No	Measured value		σ_p	σ_m	p	r_y	r_x	$\bar{r}$	$\bar{r}_a$	Predicted value	
	σ_y	σ_x								σ_y	σ_x
69	0.190	0.250	3.155	0.357	0.526	0.946	0.905	0.867	0.909	0.391	0.453
70	0.480	0.230	2.999	0.304	0.500	0.943	0.909	0.903	0.946	0.315	0.360
71	0.340	0.340	3.000	0.340	0.500	0.959	0.945	0.954	1.000	0.331	0.349

Fig. 20 The grouted soil samples for providing the measured UCS data in Fig. 18

Appendix 2

See Table 4, Fig. 21.

Table 4 Calculation details of Fig. 16

Rock proportion	Grout proportion	$\bar{r}$	$\overline{S}_{meso}$	K	Converted rock proportion	Equivalent skeleton	Predicted UCS	Measured UCS
0.11	0.40	0.97	0.07	0.56	0.06	0.42	0.18	0.14
0.11	0.28	0.96	0.09	0.37	0.04	0.29	0.08	0.05
0.11	0.50	0.96	0.09	0.71	0.08	0.53	0.36	0.36
0.11	0.35	0.97	0.07	0.47	0.05	0.36	0.13	0.12
0.11	0.46	0.95	0.11	0.64	0.07	0.48	0.27	0.23
0.19	0.38	0.97	0.07	0.52	0.10	0.41	0.17	0.24
0.19	0.26	0.96	0.09	0.33	0.06	0.27	0.07	0.05
0.19	0.52	0.96	0.09	0.73	0.14	0.56	0.44	0.44
0.19	0.34	0.97	0.07	0.46	0.09	0.36	0.13	0.16
0.19	0.45	0.95	0.11	0.63	0.12	0.49	0.28	0.26
0.26	0.37	0.97	0.07	0.50	0.13	0.40	0.16	0.23
0.26	0.28	0.96	0.09	0.36	0.10	0.30	0.08	0.11
0.26	0.50	0.96	0.09	0.70	0.18	0.55	0.42	0.49
0.26	0.34	0.97	0.07	0.46	0.12	0.37	0.13	0.14
0.26	0.44	0.95	0.11	0.61	0.16	0.48	0.28	0.28
0.34	0.37	0.97	0.07	0.51	0.18	0.43	0.20	0.21
0.34	0.25	0.96	0.09	0.32	0.12	0.29	0.08	0.11
0.34	0.53	0.96	0.09	0.74	0.26	0.60	0.58	0.61
0.34	0.34	0.97	0.07	0.46	0.17	0.39	0.16	0.30
0.34	0.46	0.95	0.11	0.65	0.23	0.53	0.37	0.58
0.41	0.38	0.97	0.07	0.53	0.25	0.48	0.26	0.28
0.41	0.27	0.96	0.09	0.35	0.19	0.35	0.12	0.15
0.41	0.53	0.96	0.09	0.75	0.32	0.64	0.71	0.83
0.41	0.34	0.97	0.07	0.46	0.23	0.43	0.20	0.25
0.41	0.43	0.95	0.11	0.60	0.27	0.53	0.36	0.42
0.49	0.41	0.97	0.07	0.58	0.35	0.56	0.43	0.51
0.49	0.27	0.96	0.09	0.35	0.27	0.41	0.17	0.22
0.49	0.55	0.96	0.09	0.77	0.41	0.69	0.97	1.04
0.49	0.38	0.97	0.07	0.52	0.33	0.52	0.34	0.41
0.49	0.43	0.95	0.11	0.60	0.35	0.57	0.48	0.53
0.56	0.39	0.97	0.07	0.53	0.41	0.58	0.50	0.49
0.56	0.29	0.96	0.09	0.38	0.36	0.49	0.28	0.27
0.56	0.55	0.96	0.09	0.77	0.48	0.72	1.16	1.36
0.56	0.32	0.97	0.07	0.42	0.37	0.52	0.33	0.36
0.56	0.42	0.95	0.11	0.59	0.43	0.61	0.61	0.53
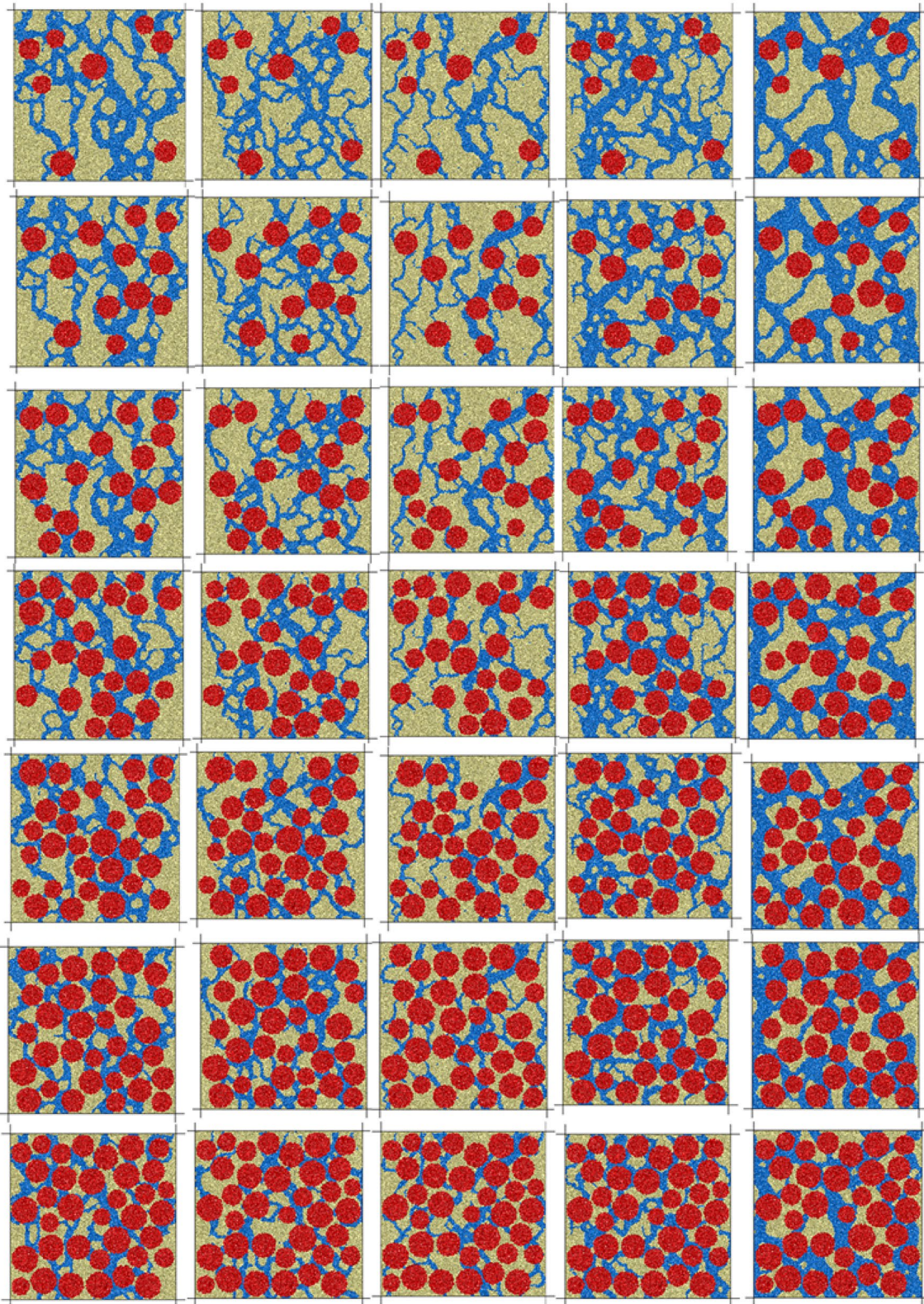
Fig. 21 The grouted SRM samples for providing the measured UCS data in Fig. 16

References

Axelsson M, Gustafson G, Fransson A (2009) Stop mechanism for cementitious grouts at different water-to-cement ratios. Tunn Undergr Sp Technol 24(4):390–397

Chen L, Yang Y, Zheng H (2018) Numerical study of soil-rock mixture: generation of random aggregate structure. Sci China-Technol Sci 61(3):359–369. https://doi.org/10.1007/s11431-017-9136-9

Coli N, Berry P, Boldini D (2011) In situ non-conventional shear tests for the mechanical characterisation of a bimrock. Int J Rock Mech Min Sci 48(1):95–102. https://doi.org/10.1016/j.ijrmms.2010.09.012

Coli N, Boldini D, Bandini A, Lopes DS (2012) Modeling of complex geological rock mixtures under triaxial testing conditions. In: ISRM international symposium—EUROCK 2012, Stockholm, Sweden. International Society for Rock Mechanics and Rock Engineering, p 12

Dong Y (2007) Experimental study on intensity character of rock-soil aggregate mixture. Rock Soil Mech 38(1):1260–1274. https://doi.org/10.1007/s11747-006-0011-3 (**in Chinese**)

Gao WW, Gao W, Hu RL, Xu PF, Xia JG (2018) Microtremor survey and stability analysis of a soil-rock mixture landslide: a case study in Baidian town, China. Landslides 15(10):1951–1961. https://doi.org/10.1007/s10346-018-1009-x

Grotenhuis RT (2004) Fracture grouting in theory; modelling of fracture grouting in sand. Civ Eng Geosci

Hamidi A, Salimi N, Yazdanjou V (2011) Shape and size effects of gravel particles on shear strength characteristics of sandy soils. Geosciences 20(80):189–196. https://doi.org/10.1201/9780203885284-c50

Han JJ, Liu BX, Zhang DL (2011) Stability analysis of S-RMS under seismic loading. Adv Mater Res 261–263:1336–1340. https://doi.org/https://doi.org/10.4028/www.scientific.net/amr.261-263.1336

Hu XL, Zhang H, He CC, Zheng WB (2018) Breakage effect of soft rock blocks in soil-rock mixture with different block proportions. In: Proceedings of China-Europe conference on geotechnical engineering. Springer, Cham, pp 809–813. https://doi.org/https://doi.org/10.1007/978-3-319-97112-4_181

Irfan TY, Tang KY (1993) Effect of the coarse fractions on the shear strength of colluvium. Geotechnical Engineering Office Civil Engineering Dept, Hong Kong

FINLAND, International Society for Rock Mechanics, Pergamon (1981) https://doi.org/10.1016/B978-0-08-027587-1.50018-5

Itasca (2016) PFC manual, version 5.0, Minneapolis

Jiang JQ, Yang GL (2010) Field tests on mechanical characteristics and strength parameters of red-sandstone. J Cent S Univ Technol 17(2):381–387. https://doi.org/10.1007/s11771-010-0056-9

Jin L, Zeng YW, Xia L, Ye Y (2016) Experimental and numerical investigation of mechanical behaviors of cemented soil-rock mixture. Geotech Geol Eng 35:337–354. https://doi.org/10.1007/s10706-016-0109-4

Jin L, Zeng YW, Ye Y, Li JJ (2017) Improving three-dimensional DEM modeling methods for irregularly shaped particles and their assembly. Chin J Geotech Eng 39(7):1273–1281. https://doi.org/10.11779/CJGE201707014 (**in Chinese**)

Kalender A, Sonmez H, Medley E, Tunusluoglu C, Kasapoglu KE (2014) An approach to predicting the overall strengths of unwelded bimrocks and bimsoils. Eng Geol 183:65–79. https://doi.org/10.1016/j.enggeo

Khorasani E, Amini M, Hossaini MF, Medley E (2019) Statistical analysis of bimslope stability using physical and numerical models. Eng Geol 254:13–24. https://doi.org/10.1016/j.enggeo

Li SC, Liu RT, Zhang QS, Zhang X (2016) Protection against water or mud inrush in tunnels by grouting: a review. J Rock Mech Geotech Eng 8(5):753–766

Lindquist ES (1994) The strength and deformation properties of mélange (Ph.D. Thesis) University of California, Berkeley

Lindquist ES, Goodman RE (1994) The strength and deformation properties of a physical model mélange. In: Proc. 1st North American rock mech. symp., Austin, Texas, pp 843–850.

Liu RT, Zheng Z, Li SC, Zhang QS (2019) Study on Grouting penetration in soil rock mixture and the mechanical behavior after grouting reinforcement. J Test Eval. https://doi.org/10.1520/JTE20170761

Nguyen NHT, Bui HH, Nguyen GD, Kodikara J (2017) A cohesive damage-plasticity model for DEM and its application for numerical investigation of soft rock fracture properties. Int J Plast 98:175–196

Potyondy D, Cundall P (2004) A bonded-particle model for rock. Int J Rock Mech Min Sci 41:1329–1364

Raymond LA (1984) Classification of melanges. In: Raymond LA, Boulder LA (eds) Melanges: their nature, origin and significance. Geology Society of America, Boulder, pp 7–20

Saada Z, Canou J, Dormieux L, Dupla JC, Maghous S (2005) Modelling of cement suspension flow in granular porous media. Int J Numer Anal Meth Geomech 29(7):691–711

Saadat M, Taheri A (2019) A numerical approach to investigate the effects of rock texture on the damage and crack propagation of a pre-cracked granite. Comput Geotech 111:89–111

Shang YJ, Xue JH, Wang SJ, Yang ZF, YangJ, (2004) A case history of Tunnel Boring Machine jamming in an inter-layer shear zone at the Yellow River Diversion Project in China. Eng Geol 71(3–4):199–211. https://doi.org/10.1016/S0013-7952(03)00134-0

Sonmez H, Altinsoy H, Gokceoglu C, Medley E (2006) Considerations in developing an empirical strength criterion for bimrocks. In: 4th Asian rock mechanics symposium

Widmann R (1996) International society for rock mechanics commission on rock grouting. Int J Rock Mech Min Geomech Abstr 33(8):803–847

Xu WJ (2008) Study on Meso-Structural Mechanics (M-SM) Characteristics and Stability of Slope of Soil-Rock Mixtures (S-RM). PhD thesis. Institute of Geology and Geophysics, Chinese Academy of Science, Beijing (**in Chinese**)

Xu WJ, Hu RL, Tan RJ (2007) Some geomechanical properties of soil-rock mixtures in the Hutiao Gorge area, China. Geotechnique 57(3):255–264. https://doi.org/10.1680/geot.2007.57.3.255

Xu WJ, Xu Q, Hu RL (2011) Study on the shear strength of soil–rock mixture by large scale direct shear test. Int J Rock Mech Min Sci 48(8):1235–1247. https://doi.org/10.1016/j.ijrmms

Xu WJ, Li CQ, Zhang HY (2015) DEM analyses of the mechanical behavior of soil and soil-rock mixture via the 3D direct shear test. Geomech Eng 9(6):815–882. https://doi.org/10.12989/gae.2015.9.6.815

Xu WJ, Hu LM, Gao W (2016) Random generation of the meso-structure of a soilrock mixture and its application in the study of the mechanical behavior in a landslide dam. Int J Rock Mech Min Sci 86:166–178. https://doi.org/10.1016/j.ijrmms

Xu WJ, Wang S, Zhang HY, Zhang ZL (2016b) Discrete element modelling of a soilrock mixture used in an embankment dam. Int J Rock Mech Min Sci 86:141–156. https://doi.org/10.1016/j.ijrmms

Zhang ZL, Xu WJ, Xia W, Zhang HY (2016b) Large-scale in situ test for mechanical characterization of soil-rock mixture used in an

embankment dam. Int J Rock Mech Min Sci 86:317–322. https://doi.org/10.1016/j.ijrmms

Zhang HY, Xu WJ, Yu YZ (2016a) Numerical analysis of soil-rock mixture's mesomechanics based on biaxial test. J Cent South Univ 23:685–700. https://doi.org/10.1007/s11771-016-3114-0

Zhang P, Jin L, Du XL, Lu DC (2018) Computational homogenization for mechanical properties of sand cobble stratum based on fractal theory. Eng Geol 232(8):82–93. https://doi.org/10.1016/j.enggeo

Zheng Z, Liu RT, Zhang QS (2019) Numerical simulation and risk assessment of water inrush in a fault zone that contains a soft infill. Mine Water Environ 38:667–675. https://doi.org/10.1007/s10230-019-00621-5

Zheng Z, Liu RT, Li SC, Yang HL (2020) Control of ground uplift based on flow-field regularity during grouting in fracture with flowing groundwater. Int J Geomech 20(3):1–14. https://doi.org/10.1061/(ASCE)GM.1943-5622.0001610